1-1-2020

Conformation And Binding Aspects Of Sulfated Carbohydrates By Liquid-State Nmr

William Vignovich

CONFORMATION AND BINDING ASPECTS OF SULFATED CARBOHYDRATES BY LIQUID-STATE NMR

A Thesis
Presented for the
Master of Science in Pharmaceutical Sciences

Department of BioMolecular Sciences
Division of Pharmacognosy
The University of Mississippi

William Pane Vignovich
May 2020

ABSTRACT

Liquid-state NMR has long been an important tool for understanding the conformations and interactions of biomacromolecules. To date these conclusions have primarily been focused upon nucleotides and peptides with little information regarding the conformational structures of carbohydrates. Through the methods described in this manuscript the conformational analysis of a sulfated fucan from *Lytechinus variegatus* has been assessed. This was achieved through a combination of NOESY spectroscopy and assessment of chemical exchange in hydroxyl protons undergoing fast chemical exchange with excess solvent. This is accomplished through usage of super-cooled H_2O:acetone solvent and T1 inversion recovery. This methodology was optimized in L-fucose and applied to the sulfated fucan for normalization of NOE information for derivatization of distance restraints. Molecular dynamics modeling further confirmed these structures as supported. Furthermore, the structure-activity relationships between glycosaminoglycan oligosaccharides and their binding partners have been heavily studied. Usage of saturation transfer difference NMR has allowed robust conclusions towards understanding the impact of chain length, position of sulfates, and carbohydrate composition on the complex formation between the sulfated polysaccharides and their binding partners.

LIST OF ABBREVIATIONS

NMR	Nuclear Magnetic Resonance
GAG	Glycosaminoglycan
SAR	Structure-Activity Relationship
ppm	Parts Per Million
HSQC	Heteronuclear Single Quantum Coherence
NOESY	Nuclear Overhauser Effect Spectroscopy
NOE	Nuclear Overhauser Effect
trNOE	Transferred Nuclear Overhauser Effect
ROESY	Rotating Frame Overhauser Effect Spectroscopy
COSY	Correlation Spectroscopy
TOCSY	Total Correlation Spectroscopy
T1IR	T1 Inversion Recovery
STD	Saturation Transfer Difference
STDD	Saturation Transfer Double Difference
STD-HSQC	Saturation Transfer Difference-Heteronuclear Single Quantum Coherence
STD-HMQC	Saturation Transfer Difference-Heteronuclear Multiple Quantum Coherence
FID	Free Induction Decay
Hp	Heparin
HS	Heparan Sulfate
CS	Chondroitin Sulfate

DS	Dermatan Sulfate
KS	Keratan Sulfate
HA	Hyaluronic Acid
MW	Molecular Weight
HBP	Heparin Binding Protein
CCL5	C-C Motif Chemokine Ligand 5
MK	Midkine
IL-10	Interleukin-10
LAR	Leukocyte Common Antigen-related
CXCL12α	GBP Stromal Cell-derived Factor-1 alpha
FGF-2	Fibroblast Growth Factor 2
FGF-10	Fibroblast Growth Factor 10
AT	Antithrombin

ACKNOWLEDGEMENTS

I would like to extend my sincere gratitude to Dr. Vitor Pomin for the opportunity to take on these challenges I have experienced in my time at Ole Miss. In addition to providing me with a foundation of knowledge in Nuclear Magnetic Resonance through his coursework his trust in my ability to solve problems and providing advice and clarification as needed has been pivotal in my development as a scientist. Through my time here I have gained a clear understanding of the importance of glycobiology and NMR and its impact and potential.

I would also like to thank my labmates Alysia and Rohini for being patient with me during times of stress and for the level of teamwork that we have accomplished in the laboratory while working together. Without sharing knowledge with each other and even minor assistances our work would be greatly hindered.

An extension of gratitude is also due to Dr. Joshua Sharp and his group for their graciousness and openness to share towards our budding group. I would like to especially thank Dr. Charles Mobley for his patience and consistently being a source of information on various aspects of science and proper laboratory techniques during this time.

Then, once more, a final thank you to the department of Biomolecular Sciences and my graduate program coordinator Dr. Cole Stevens, department chair Dr. Willett, and Sherrie, Danielle, and Candace for their constant assistance and keeping things running so smoothly for us. And of course all of the students and post-docs within it who so freely share their success, struggles, and knowledge.

TABLE OF CONTENTS

LIST OF FIGURES

LIST OF TABLES

CHAPTER 1. NUCLEAR MAGNETIC RESONANCE

1.1 NUCLEAR MAGNETIC RESONANCE

Nuclear magnetic resonance (NMR) has been a staple in structure elucidation of small and large molecules since its inception in the mid 1900s by Bloch and Purcell's groups. Awarding the Nobel Prize in Physics in 1952 (1). While originally optimized for the purpose of elucidation of small molecules with high proficiency especially in comparison to older methods like infrared spectroscopy, the field of NMR has expanded greatly through the last decades in regards to its application in large molecules. Among its current uses are solution structures of biological macromolecules beyond 1000 kDa (2) and interactions of these macromolecules in solution. In addition to this NMR has seen great usage in understanding reaction rates (3), metabolomics (4), and structure-activity relationships (SAR) (5). Despite its diversified usage NMR is still considered a low sensitivity technique with much higher sample preparations than other analytical techniques.

In theory the concept of NMR is based upon the observation of specific precession patterns of individual nuclei when submitted to a strong external magnetic field. The resultant data undergoes Fourier transformation, changing time domain to frequency domain. The resultant information is a spectrum which displays peaks at specific values and patterns. These are called chemical shift and *J*-coupling, respectively. These specific precession patterns observed are referred to as Larmor frequencies. Larmor frequency is dependent upon the external

magnetic field, conventionally named B_0. Resolution of this information is highly dependent on the intensity of the B_0 (400 Mhz, 600 MHz, 800 MHz) where high magnetism increases sensitivity. In addition to magnetic field advances in hardware such as cold and cryo probes have also been employed to increase sensitivity (6).

Atomic nuclei that can be manipulated and therefore observed through NMR spectroscopy are nuclei whose spin quantum number is equal to ½. This requirement is due to the necessity of a lower energy state that can absorb the additional radiation sequestered by the pulse to switch this low energy state to the high energy state. This heavily limits the amount of atoms that can be observed through NMR with few atoms being naturally abundant in spin-half nuclei. Common nuclei observed through NMR are nitrogen 15, carbon 13, fluorine 19, and hydrogen 1. Of these four nuclei only ^{19}F and ^{1}H are in high natural abundance. Samples containing ^{15}N and ^{13}C often must be atomically labeled to overcome a severe lack of sensitivity due to low natural abundance for studies of molecules where these atoms are important to be observed. This is especially relevant in studies involving biological macromolecules where the goal is to identify the position or changes within amide resonances.

Data from NMR spectroscopy can be observed within multiple dimensions. For many applications NMR is presented in one dimension. However when the molecule of interest is complicated or other structural features are probed then data acquisition in multiple dimensions is often required. While usually conducted in 2 dimensions, this is not the limit with >2 dimensional NMR experiments can be conducted as well (7). In 1D NMR the single axis is limited to observation of a single species of nuclei of different frequencies. Among those discussed, observation of ^{1}H, ^{13}C, and ^{19}F are those routinely utilized in organic chemistry. ^{1}H NMR is undoubtedly the most heavily used NMR experiment of these. Within these spectra there

are two primary figures of merit that are often observed that contain a wealth of information. These two sources of information are chemical shift and *J*-coupling. These will be discussed in more detail further.

2 dimensional approaches are either homonuclear, a single type of nuclei, or heteronuclear, multiple nuclei in interaction with one another (ex. ^{1}H-^{15}N HSQC). For purposes of structure elucidation both approaches are often used to compile structural information about the molecule that is being observed. Homonuclear information allows for more in depth probing of nuclei and neighbors within the same species. While heteronuclear NMR allows for understanding nuclei of different species. This is especially important in the context of biopolymers that are usually very large or hard to observe. In proteins for instance ^{15}N is observed in interaction with solvent protons to understand amide resonances or ^{13}C to probe peptide backbones (8). While ^{31}P in addition to ^{15}N nuclei find usage in studies involving nucleotides (9)(10). However carbohydrates are limited in that they do not contain another species of nuclei outside of ^{13}C and ^{1}H to extract information from through NMR. In the observation of biomacromolecules these dimensions are dominated heavily by heteronuclear data for the purposes of both structure elucidation and interactions of these larger molecules either with ligands (11)(12) . Or other variables like solvent and temperature that can be experimentally altered to probe the properties of these complex systems and polymers (13)(14).

1.1.1 CHEMICAL SHIFT

Of the two most important observables in NMR spectroscopy is chemical shift. In simple terms this is the value that a peak corresponds to within the NMR spectrum. Chemical shift values are calculated as a part per million (ppm) scale. In NMR, ppm corresponds to a

standardized measurement to describe Larmor frequencies of specific nuclei in the spectrum as related to the frequency at which they precess at. This relationship is described by the equation ppm = (actual frequency - B_0)/B_0. Through this equation, frequencies measured in hertz can be easily converted to a reproducible value in ppm regardless of B_0. This allows for uniform data of the same sample under different magnetic fields assuming other variables remain consistent. Different nuclei do not provide the same values for chemical shift ppm information, giving rise to different chemical shift ranges or scales for the different isotopes.

Chemical shift values are determined by a myriad of different factors. Among these are temperature and chemical environment. Temperature may have an impact upon the ppm value of a specific proton in solution NMR. The heavily studied nuclei are those within water that exhibit this perturbation in chemical shift due to fluctuations in temperature. For this purpose this proton can be observed in different conditions to map the change in temperature (15). This phenomenon is not only limited to water protons, nor protons in general but can be traced in other novel applications as well (16). Of particular importance in temperature impact on chemical shift is within peptides whose tertiary structure leads specific NMR signals and chemical shift locations. Upon alteration of the temperature-dependent conformation of the peptide can cause a shift within the resultant NMR spectrum that can be diagnostic for structural assessment (17). Within the structural biology of nucleotides this phenomenon is also explored (18)

Patterns of chemical shifts in regards to functional groups are well described but are not rules. For example methyl protons often fall around 1 ppm however they are often observed from -1 ppm up to ~1.5 ppm. Differences in chemical shift values reflect these differing chemical environments and neighboring nuclei. Strongly electronegative atoms in proximity to observable nuclei will exert an effect where these nuclei will be observed downfield. This is due to nuclei

being electronically deshielded or shielded. The concept of shielding can be best described as an increase in electron density surrounding a nucleus. In deshielding this is the opposite relationship where a decrease in electron density reduces the magnetic effects upon the nucleus (19)(20). Functional groups containing heavily electronegative atoms induce heavy deshielding resulting in a downfield displacement of signal frequency (ppm) of the observed nuclei. This is exceptionally clear in hydroxyl and amide resonances that are often probed in NMR studies (21)(22). Another aspect of the chemical environment surrounding the nucleus is also playing a role in the precession of the nuclei. Common molecular properties like hydrogen bond length can also produce an impact on the observed chemical shift (23) as can solvent assuming the experiment is performed in solution-state NMR (24).

.

1.1.2 *J*-COUPLING

J-coupling is a description of the patterns observed in NMR spectra when protons are near each other. These interactions are due to magnetic dipole moments occurring in electrons due to the influence of the B_0. In protons this is usually, but not always, observed between vicinal carbon-bound protons. The splitting pattern follows the n+1 rule where n is the number of neighboring signals plus the single peak from the original signal. This phenomenon results in the NMR spectrum displaying predictable patterns of multiplets. These can be, but are not limited to, a doublet, which has one neighboring signal, a triplet, 2 neighboring signals, and a doublet of triplets, when a doublet is further split into a triplet. Through further analysis the distance of these peaks can be converted to atomic distances between nuclei. Working with *J*-coupling allows for interesting conclusions within NMR. Specific properties in physical chemistry can be understood through this property. Among these advantages is understanding the impacts of lone

pair electrons (25), hydrogen bonding interactions (26), as well as producing patterns for preliminary database information that can be used in metabolomics (27).

1.1.3 T1 AND T2 RELAXATION PROPERTIES

Following magnetization of the compound of interest there is a relaxation period in which the nuclei equilibrate to the external magnetic field, B0. These are named T1 and T2 spin relaxation times.

T1 relaxation, or spin-lattice relaxation, is the relaxation that is due to the protons being observed relaxing in regards to the magnetic field B_0 (28). T1 values observed often follow a pattern within the chemical properties of the nuclei being observed (29). Within a clinical setting T1 relaxation is the property in which magnetic resonance imaging is observed. Within this setting different biomacromolecules such as lipids (30) and bone tissue (31) provide varying but somewhat predictable T1 relaxation times that can be used to image organs. Through this methodology different diseases states such as leukemia and liver functionality are also elucidated through this property in application towards magnetic resonance imaging (32)(33). This comparison is also observed within small and large molecules where observations of these relaxations are different depending upon the chemical environment in which the observed nuclei is in.

T2 relaxation, or spin-spin relaxation, is transverse relaxation of nuclear precession within the external magnetic field. This value is always less than that of T1. T2 is the transverse-spin relaxation time which is dependent on how the magnetization of the different nuclei interact and influence the precession of each other after a 90 degree pulse that flips the nuclear spins to the x-y quadrature. This flip is necessary for NMR signal acquisition. The longer the nuclear spin

remains with its magnetization projection on the quadrature, the longer the T2 values. Determination and analysis of the T2 values are important to understand how the magnetic field is influencing the spin dynamics of the observed molecule under NMR investigation. Overall, T1 and T2 spin relaxation values are parameters used to understand overall dynamics of the molecules in solution or specific internal motions of certain chemical groups.

1.1.4 PULSE SEQUENCES

Standard one dimensional data is gathered from a single 90 degree pulse followed by a data acquisition step (**Figure 1)** in which the information undergoes Fourier Transformation to yield the specific chemical shift values and *J*-coupling values and patterns that are indicative of molecular structure. There is a vast array of different pulse sequences in multiple dimensions that can be used to probe molecular structure or interactions of these molecules. Pulse sequences can be manipulated to achieve many things. Among these are selectively shaped pulses as can be seen in saturation transfer difference (34), the specific excitement of particular nuclei and transfer of spin in experiments like heteronuclear single quantum coherence (HSQC) spectrum (35) and cross-polarization transfer experiments, as seen in Nuclear Overhauser Effect Spectroscopy (NOESY) spectra analyzed within different mixing times.

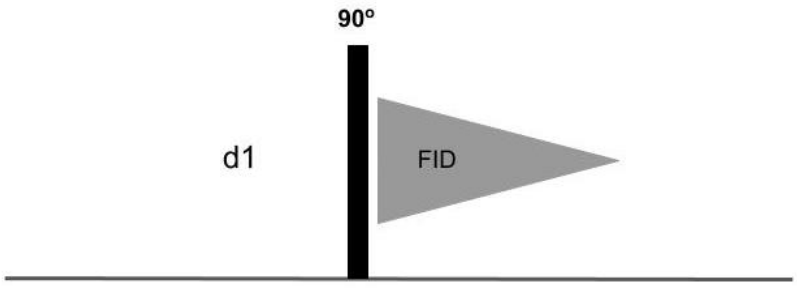

Figure 1: The standard 1D NMR pulse sequence for a single scan. d1 corresponds to the initial relaxation period following acquisition of the free induction decay (FID) to allow for the sample to re-homogenize with B_0. 90 degree pulse is a hard RF pulse to allow for precession of the nuclei. FID corresponds to the period of time in which information is recorded by the spectrometer.

1.2 MOLECULAR CONFORMATION OF BIOMACROMOLECULES THROUGH NMR

Molecular conformation of molecules in 3D space can be accomplished through NMR and is well developed and in widespread use. While there is an abundance of information in regards to the structures of peptides and nucleotides in solution there is not the same level of abundance of carbohydrate studies. Atomic distances through NMR are mainly probed through *J*-coupling values and information from signals of nuclear overhauser effects (NOEs). In comparison to other methods NMR has the advantage of being in solution. Solution state NMR allows for understanding the conformation of molecules in or as close to physiological conditions as sample preparation allows.

1.2.1 ATOMIC DISTANCE THROUGH *J*-COUPLING

J-coupling values describe distance of bonds in addition to the number of neighboring protons as was stated. Distance of neighbors can be described as the distance between peaks as measured in hertz. This value is independent of the external magnetic field but dependent on the pattern of neighboring NMR sensitive nuclei of the observed nucleus under investigation.

1.2.2 NUCLEAR OVERHAUSER EFFECT

Nuclear overhauser effect spectroscopy (NOESY) is the observation of an interaction of two spin-half nuclei that transfer magnetization through space. In **Figure 2** the pulse sequence for the NOESY experiment can be seen. Within this pulse sequence the delay in the pulse sequence corresponding to mixing time must be optimized. This allows for optimal cross polarization of the nuclei as too short of a mixing time will not allow this polarization to reach a maximum intensity or too long and the cross polarization event will be fully relaxed producing low or nonexistent signals. This is necessitated by the different transverse relaxation times of different protons with variable molecules (63). This intensity is also dependent upon the temperature the experiment is run at. Therefore in conformational studies this mixing time must also be optimized per temperature if variable temperatures are used (64).

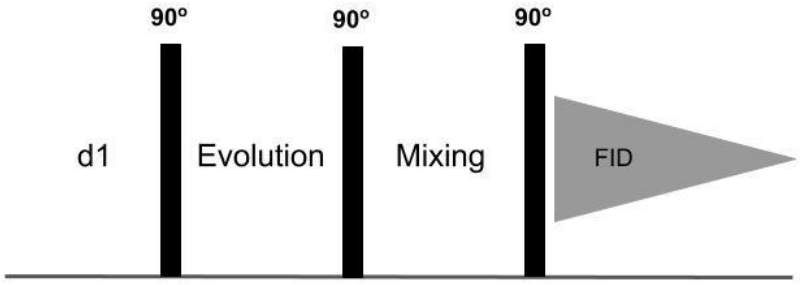

Figure 2: The standard NOESY pulse sequence is shown. d1 corresponds to a relaxation period after the acquisition of the FID in which the sample homogenizes with the external magnetic field. This is followed by a 90 degree pulse to the sample followed by an evolution period in which the nuclei freely interact. Following this evolution period is a 90 degree pulse followed by a 90 degree pulse. The mixing time period is the period of time in which magnetization is transferred between nuclei. This is followed by free induction decay (FID) for acquisition.

Within the realm of understanding conformation of molecules in space through NMR NOE has been the subject of this for decades. Calculation of atomic distances through peak volume is a means to determine conformations with an accuracy of ± 5 angstroms in comparison to other methods (65). The distance between two nuclei can be calculated from the peak volume within the NMR spectrum following a similar $1/r^6$ value. This phenomenon will be further explained within the next chapter.

CHAPTER 2. GLYCOBIOLOGY

2.1 SULFATED CARBOHYDRATES

Glycobiology is an interdisciplinary science regarding the functional and structural analysis of carbohydrates. Common tools within this body of research include NMR, Mass spectrometry, chromatography, and biological assays.

Within the last few decades the science around understanding carbohydrates has accelerated immensely (36). The scientific initiative named Glycomics has been created and conclusions derived from related research has proved pivotal to understanding many aspects of carbohydrate impact in physiology (37). While previously considered heavily for metabolic importance and related to energy storage, the understanding of complex carbohydrates in signaling and structural functions is profound and seems to be crucial to an incredibly diverse set pathophysiological events in multicellular organisms. While being crucial in maintaining functional integrity within cells as proteoglycans and cell wall components in eukaryotes (38) and prokaryotes (39) these molecules also have direct effects upon a vast array of biological systems at all levels of life (40). Among these are inflammatory responses and other tissue impacts (41)(42), tumorigenesis (43), neurological effects (44), as well as being heavily explored for anticoagulative effects (45).

In glycobiology, many biologically active glycoconjugates exist at the extracellular matrices and surround the coat surface of the cells (glycocalix). Among all these glycoconjugates are N- and/or O-linked glycoproteins, glycolipids and proteoglycans. Of particular importance in

this research are the glycosaminoglycans (GAGs) and other sulfated polysaccharides. GAGs are composed of an uronic acid or neutral sugar, galactose (Gal) linked to an amino sugar (46). This is presented as alternation disaccharide units of the hexuronic acid and hexosamine constituents. Monomers that can be present within this group of carbohydrates are glucuronic acid or iduronic acid as the hexuronic acid and N-acetylglucosamine or N-acetylgalactosamine as the hexosamine (46). The four major groups of GAGs are observed in **Figure 3.** R groups determine the location in which sulfation of the original hydroxyl group can be the chemical substituent.

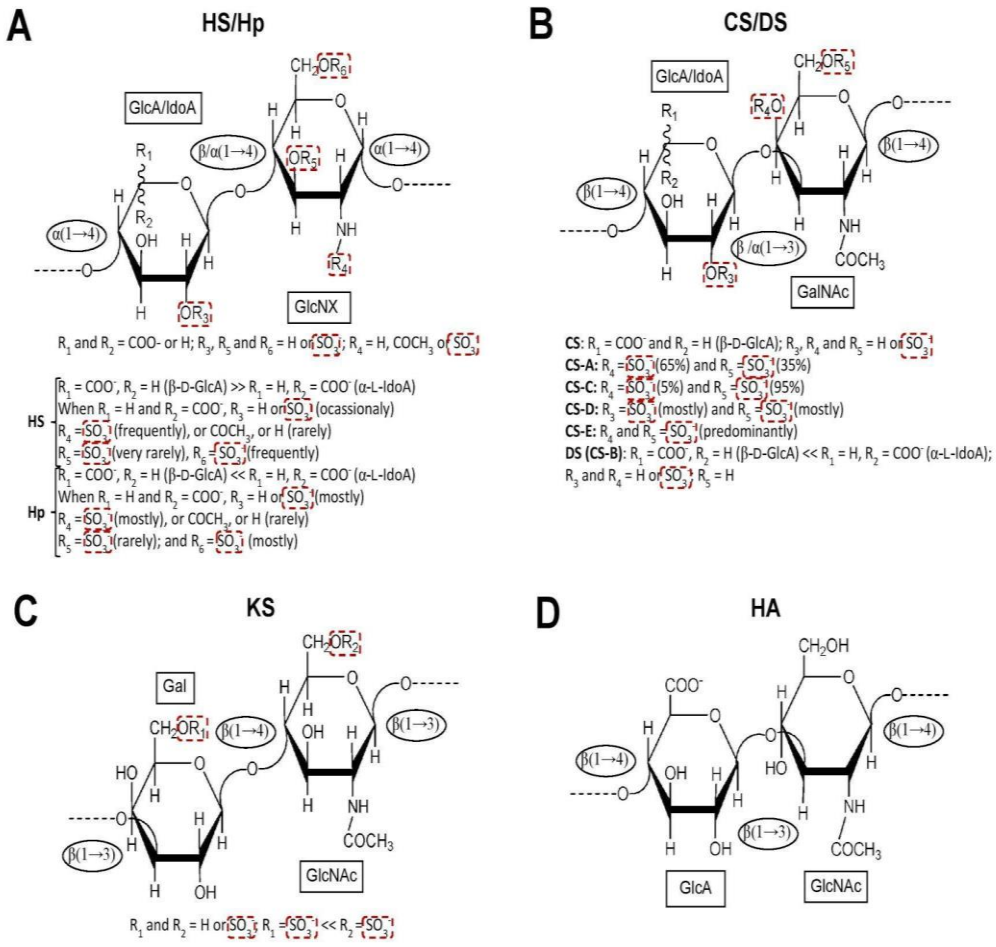

Figure 3: Representations of the 4 major types of GAG repeating disaccharide units. R groups represent hydroxyl residues in which sulfation can occur. In A, heparin (Hp) and heparan sulfate

(HS) is composed of a uronic acid linked to α-glucosamine in repeating [1-4] linkages. In B, chondroitin sulfate (CS) and dermatan sulfate (DS) is composed of alternating [1-4] linked glucuronic acid with [1-3] linkage to a N-acetylgalactosamine. Dermatan sulfate is a similar structure but containing an iduronic acid. Species of CS/DS are determined through sulfate positions within the disaccharide. In C, keratan sulfate (KS) is composed of repeating [1-3] linked galactosamine with [1-4] linkage to N-acetylglucosamine. In D, hyaluronic acid (HA) is the only non-sulfated unit. These are composed of repeating [1-4] linked glucuronic acid with [1-3] to N-acetylglucosamine.

Briefly, keratan sulfate is a sulfated polysaccharide that is observed to be expressed within brain cells as well as corneal tissues. This GAG functions as a proteoglycan (47). Hyaluronate is an important component of extracellular matrices and is the only member of this family that is not sulfated at any position. Hyaluronate is an incredibly large polysaccharide as well, with observed molecular weights (MW) being ~100. In addition to being present in the ECM of cells it is also prevalent in synovial fluids (48) and has been explored for its usage in pain relief (49) as well as other functions like dendritic modulation (50). Chondroitin sulfates are highly expressed in cartilaginous tissues, synovial fluids, and as proteoglycan components. Chondroitin sulfates exist as long chains of individual disaccharide subunits. The sulfation pattern within these disaccharides is indicative of the species of chondroitin sulfate subunit. Chondroitin sulfate is also a well studied proteoglycan whose physiological impact is also diverse with interactions in inflammation (51), neuronal implications (52), and anticoagulation (53), among others. This activity is highly variable in regards to the chondroitin sulfate composition and distribution of sulfate residues. While arguably the most highly studied, heparan

sulfate and heparin are observed as important signaling and research molecules (54). This is especially true within coagulation pathways where they are found to be an important anticoagulative drug on the market. This interaction in the coagulation cascade is due to its interactions with thrombin binding leading to its inactivation and subsequent loss of function (55). This well described function has led to a market for this sugar as a drug worth billions worldwide. Due to previous issues with contamination such as the heparin crisis of 2008 as well as its capacity for heparin induced thrombocytopenia other pharmaceutical options have been explored as alternatives. Among these other options are synthetic heparin (56) as well as sulfated carbohydrates from marine organisms (57).

2.1.2 SULFATED POLYSACCHARIDES FROM MARINE SOURCES

Marine organisms are an excellent source of novel sulfated polysaccharides. It is apparent that many of these polysaccharides suffer the same lack of structural homogeneity that the mammalian GAGs do. However in some cases there is clear evidence of homogeneous structure. This is exemplified in a sulfated fucan from the sea urchin *Lytechinus variegatus*. This organism expresses a long chain polysaccharide composed of uniform tetrasaccharide units. This tetrasaccharide units follow the uniform structure of [3)-α-L-Fucp-(2SO_3^-)-(1→3)-α-L-Fucp-(4SO_3^-)-(1→3)-α-L-Fucp-(2,4SO_3^-)-(1→3)-α-L-Fucp-(2SO_3^-)-(1→]. Regular structures are paramount in understanding the structural components that are involved in these physiological processes.

From a pharmacological perspective it has been widely observed that these sugars can exhibit similar biological action as mammalian derived GAGs. Among these are fucosylated chondroitin sulfates (58), sulfated fucans (59), and sulfated galactans (60). These unique

polysaccharides can be observed in a diverse set of organisms in both plants and animals. The anticoagulant action of these marine derived polysaccharides has been well documented with activity comparable to heparin, which is still one of the most economically relevant carbohydrate drugs on the market. In addition to proposed similar methods of action as these the potential for interactions with other proteins in the coagulation pathway has also been suggested (61). Due to this similar activity these polysaccharides provide an interesting avenue of pharmacological studies. An issue arises when trying to understand their structures and how this relates to their function. This is due to these carbohydrates often being as diverse as the organisms they are expressed in. These sugars can be linear or heavily branched (62). Due to this structural diversity the structures must be well described before probing their pharmacological effects. This highlights an excellent usage of regular carbohydrate building blocks like is seen in *L. variegatus*. This structure elucidation is primarily performed through mass spectrometry and NMR spectroscopy.

2.2 STRUCTURE ELUCIDATION OF CARBOHYDRATES THROUGH NMR

Structure elucidation through NMR can be accomplished within reason through simple 1D spectra. In carbohydrates, a general pattern is usually seen in a crowded region between 3-5 ppm where most signals appear and chemical shift degeneracy is consequently very high. Due to deshielding from the carbon-bound oxygen upon cyclization of the linear carbohydrate rings, anomeric protons can be observed furthest downfield in the ^{1}H NMR spectra. However, as molecules of interest become more structurally complex as can be seen in the carbohydrates other methods are used in combination with one another. Usage of multiple NMR experiments increased the overall integrity of conclusions found from previous experiments. This

combinatorial method is especially relevant to ring bound protons that experience intense signal overlap. Usually this is accomplished through conducting multiple 2D pulse sequences. Most commonly these methods are HSQC, COSY, TOCSY, and NOESY or ROESY.

Correlation spectroscopy (COSY) is an experiment that traces neighboring nuclei to each other allowing for elucidation of nuclei that are neighbors. To increase the number of neighbors seen by a single nucleus the usage of the total correlation spectroscopy (TOCSY) is conducted. TOCSY experiments allow for observation of through-bond interactions of more than 3 bonds in distance. This is achieved through a saturation step (spinlock) within the pulse sequence that magnetization is intermolecularly distributed through bonds. In carbohydrates this allows for observation of the spin system or characterization of a single monosaccharide unit with no impact from the glycosidic linkage between units.

Heteronuclear single quantum coherence (HSQC) experiments in regards to carbohydrates involved ^{1}H and ^{13}C nuclei directly bound. Conclusions regarded from these experiments allow for additional integrity to proton based structure elucidation.

NOESY and ROESY experiments can often be looked at as complimentary of the TOCSY experiments in regards to structural assessment of carbohydrates in solution. These experiments observe proton-proton interactions through space. In these experiments it is seen that in addition to neighboring peaks that can be observed in TOCSY the protons in adjacent sugar monomers can be observed to allow for assignment of the glycosidic linkage positions and other inter and/or intraresidue connectivities. For this purpose NOESY is a crucial tool in elucidating the location of glycosidic linkages within carbohydrate polymers and the 3D structures of both rings and chains. In tandem with TOCSY the NOESY experiment will display many of these neighboring protons as well as the proton observed between the reducing and

nonreducing ends of the monosaccharides that are glycosidically bound. In all, NOESY and ROESY experiments have added advantages in their ability to allow for understanding the 3 dimensional structure or conformation of a molecule in solution.

CHAPTER 3. CONFORMATION OF A SULFATED FUCAN FROM *LYTECHINUS VARIEGATUS*

3.1 ISOLATION AND CHARACTERIZATION OF SULFATED FUCAN FROM *L. VARIEGATUS*

Among those marine species who have been explored for possible novel sulfated polysaccharides is *L. variegatus* a sea urchin that is distributed throughout the coasts of North and South America (66). Within the reproductive processes of this sea urchin they produce a rich jelly coat surrounding their eggs. This jelly coat as well as male's seminal fluids contain highly concentrated sulfated polysaccharides (6768). While previously mentioned sulfated polysaccharides from marine sources are often branched as is seen in algae (69), this, however, is not the case for *L. variegatus* which produces a uniform linear polysaccharide within its egg jelly. Structurally this polysaccharide is composed of a fucose backbone with a regular structure (70). This regular structure enables advanced studies of conformation and dynamics.

In the manuscript titled "*Conformational properties of l-fucose and the tetrasaccharide building block of the sulfated L-fucan from Lytechinus variegatus*" by Bezerra et al. (71) we had sought to determine experimentally supported information regarding the fucan from *L. variegatus.* It is hypothesized that the exchange of hydroxyl group protons with deuterium oxide resulted in incorrect NMR based distance measurements through NOE. To assess this hypothesis

the protons needed to be both observed as NMR signals through protonation as well as understanding the rate of occupancy between solvent protons and hydroxyl protons in solution.

It was determined through NMR and mass spectroscopy that this sulfated polysaccharide exists as a repeating unit of tetrasaccharides composed of fucose. This tetrasaccharide repeated unit is pictured in **Figure 4.**

Extraction of the sulfate fucan was carried out through the methods described by Pomin et al. (72). In these methods *L. variegatus* specimens were collected and the egg jelly was separated from the organism. Following this step is purification through diethylaminoethyl cellulose weak anion exchange chromatography eluted by NaCl gradient to isolate and purify the polysaccharide. This method isolates a high molecular weight polysaccharide chain of the sulfated fucan that is unkind to NMR studies. To overcome the issue of this high molecular weight the polysaccharide was depolymerized into tetrasaccharide fragments through a mild acid hydrolysis performed in 0.01 M HCl for 1 h at 60^{o}C. This mixture was then neutralized through an equivalent molar portion of NaOH solution. Separation of this resultant mixture through size exclusion chromatography with a BioGel P-10 resin filled column yields polydisperse fragments of differing MW.

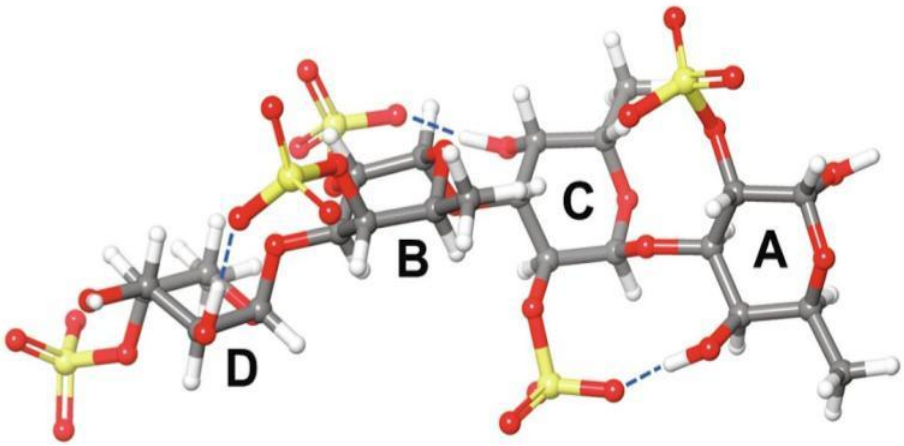

Figure 4: Repeating unit of the sulfated fucan from *Lytechinus variegatus* 3D model created by AyoOluwa Aderibigbe; blue dashed lines represent hydrogen bonds. Individual differing fucose monomers are described as D, B, C, and A. Single letter nomenclature is a result of the order of alpha anomeric protons in the downfield region of the 1D NMR spectrum where A is the most downfield signal followed B, C, and D. D, B, and A contain a single 2 or 4-sulfate. C is disulfated at positions 2 and 4. The structures and glycosidic linkages are as follows:

D: [→3)-α-L-Fucp-(2SO_3^-)-(1→]

B: [→3)-α-L-Fucp-(4 SO_3^-)-(1→]

C: [→3)-α-L-Fucp-(2,4 SO_3^-)-(1→]

A: [→3)-α-L-Fucp-(2 SO_3^-)-(1→]

Due to the homogenous structure of this tetrasaccharide unit this carbohydrate is a logical choice for developing a method to observe the conformation through NMR. This is in comparison to the famously heterogenous GAGs like heparin and chondroitin sulfates that there is much difficulty in obtaining well described structures for NMR studies.

3.2 DIFFICULTIES OF CONFORMATION OF SULFATED CARBOHYDRATES

3D solution structures of carbohydrates are vastly under studied with very few examples currently present in the literature. This is due to the structural moieties of these molecules that lead to a lack of restraints for NOE derived distance restraints which is hypothesized as the impact of solvent exchange at hydroxyl protons sites. A primary factor reducing the intensity of NOE signals observed in these carbohydrates is chemical exchange between solvent protons (or deuterons) and the carbohydrate hydroxyl groups. To assess the conformation of the sulfated fucan from *L. variegatus* the optimal conditions for calibrating the NOE peaks needed to be first understood using L-fucose as a model system.

Before this however, another aspect of the experimental design that must be assessed is the impact of rotational correlation time on the signals observed through NOE. At higher MW NOE signal becomes negative while in intermediate MW this signal is unobservable before becoming a negative value. This leads to a lack of cross-peak information and therefore relevant determination of restraints for NOE based atomic distance information. This is visualized in **Figure 5.** To overcome this issue the ROESY experiment can be performed to assure all signals are positive. NOESY and ROESY spectra were collected to determine if the NOESY experiment is optimal for fully described cross peak information. The results of this can be observed in **Figure 6.** Wherein, we observe no loss of signal between the two experiments. This is an

excellent result as it assures cross-peak information can be accurately observed Through NOESY.

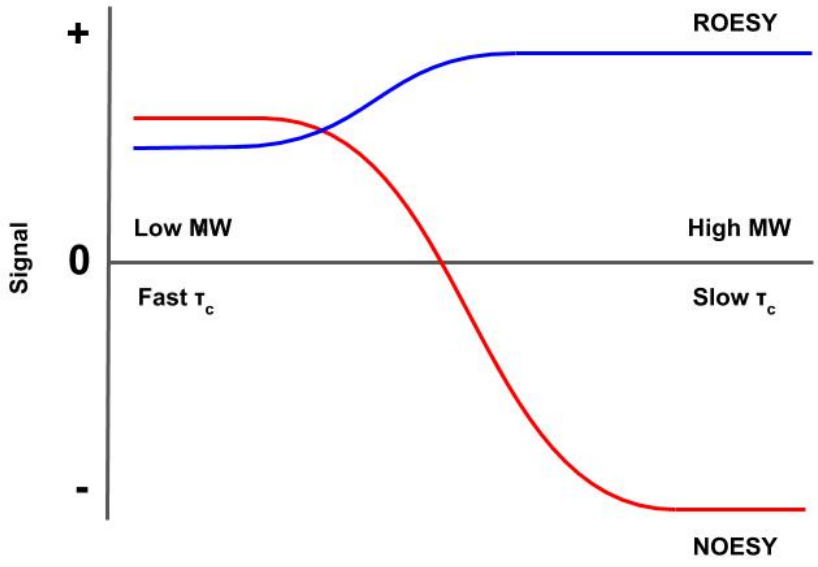

Figure 5: Representation of signal value as a function of rotational correlation time (τ_c) as it is related to molecular weight of the sample. Value of 0 represents a complete loss of NOE signal.

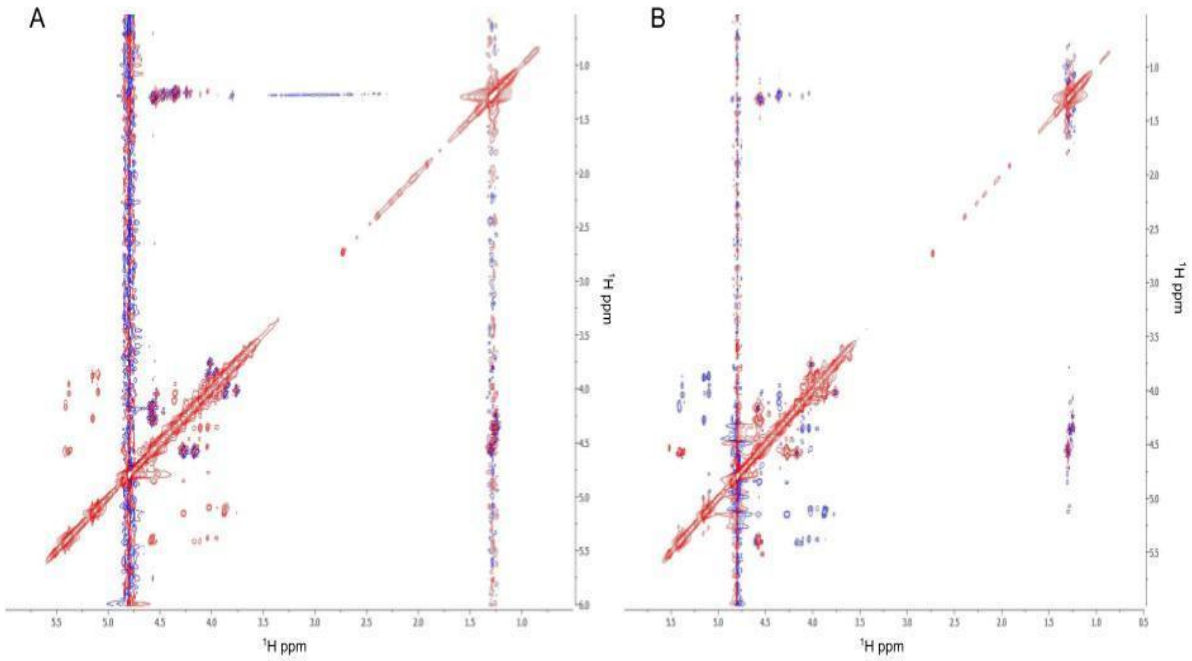

Figure 6: A comparison of NOESY vs ROESY spectra. In comparison a clear pattern of negative (red) NOE vs positive (blue) ROE is observed by the difference in phasing. Both spectra were acquired with a mixing time parameter of 25 ms.

A: NOESY spectrum acquired at 25ºC of sulfated fucan tetramer.

B: ROESY spectrum acquired at 25ºC of sulfated fucan tetramer.

3.2.1 HYDROGEN/DEUTERIUM EXCHANGE

The primary issue as stated with these structures is within the hydroxyl groups present on the sugar backbone. Hydroxyl groups contain a labile proton that readily exchanges with water protons or in the case of solution NMR spectroscopy with the deuterons in deuterium. This is a well explored concept within amino acid side chains and even solvent-solvent interactions however within carbohydrates studies utilizing this phenomenon are not common (73)(74). Chemical exchange reduces the occupancy of protons observable through NMR this is demonstrated in **Figure 7** where the phenomenon of deuterons occupying the hydroxyl group proton is represented through the two way arrow. This leads to a lack of signal within the NMR spectra under normal conditions of running NMR experiments of carbohydrates in a deuterium oxide solution at room temperature. To overcome this initial lack of signal the exchange rate needed to be slowed as well as the saturating the solvent with exchangeable protons. To accomplish this task fucose was dissolved in a mixture of H_2O and deuterated acetone at a ratio of 85:15%. This solvent mixture assures the presence of protons that can undergo exchange while deuterated acetone serves as a necessary standard for resonance signal locking. As well as a reduction of freezing point to allow for super-cooled experiments while still in the liquid phase. Freezing point is an important aspect of this observation as protons will exchange with the solvent slower at lower temperatures. Usage of super-cooled solvents in solution NMR is a reliable method to observe these exchangeable protons (75).

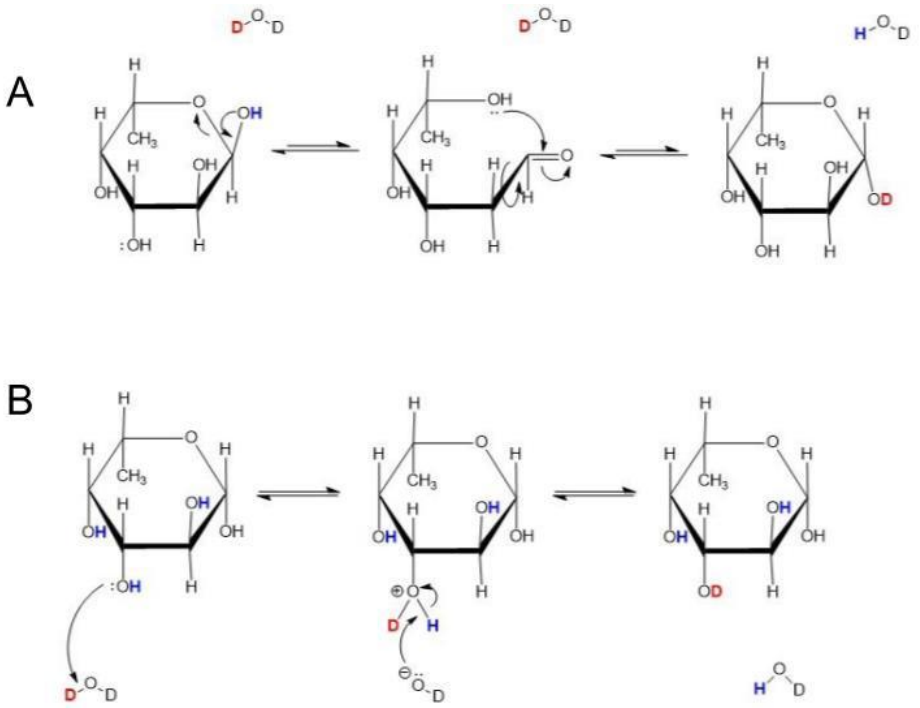

Figure 7: Example of proton chemical exchange in L-fucose with deuterium oxide. In both A and B red represents deuterons and blue represents exchangeable proton. A: Chemical exchange of anomeric proton undergoing mutarotation and chemical exchange. Arrows represent a preference in equilibrium between alpha and beta states. B: Chemical exchange of hydroxyl bound proton. All protons in blue are undergoing the similar mechanism for this exchange.

Due to the importance of maintaining the utmost structural integrity of the sulfated tetrasaccharide in this study the impact of this additional acetone needed to be understood. This was performed through a titration of increasing concentrations of acetone in the solvent mixture from 99.9% D_2O titrated to a 75:25 D_2O:acetone mixture with a 5% stepwise addition of the acetone into the solution. The result of this is pictured in **Figure 8.** In this titration, there were no notable differences in chemical shift or *J*-coupling values observed within the tetrasaccharide indicating that this additional acetone did not result in any significant changes in the observed conformation these sugars.

Demonstrated in **Figure 9,** protons within the hydroxyl groups on fucose become observable as temperature is reduced with a step size of 5^{o}C starting from 25^{o}C reduced to 5^{o}C. At the region of spectra at 5.5-8 ppm the intensity of these signals increases at reduced temperatures as well as a significant reduction in line-widths observed. It is very clear however that the reduced intensities of these residues do not equal that of carbon bound protons that are not undergoing chemical exchange within this spectrum. After confirmation of the above this methodology was repeated within the tetramer. This structure necessitated the usage of cooler temperatures. Seen in **Figure 10** the sulfated fucan was protonated at hydroxyl proton and sulfate residues.

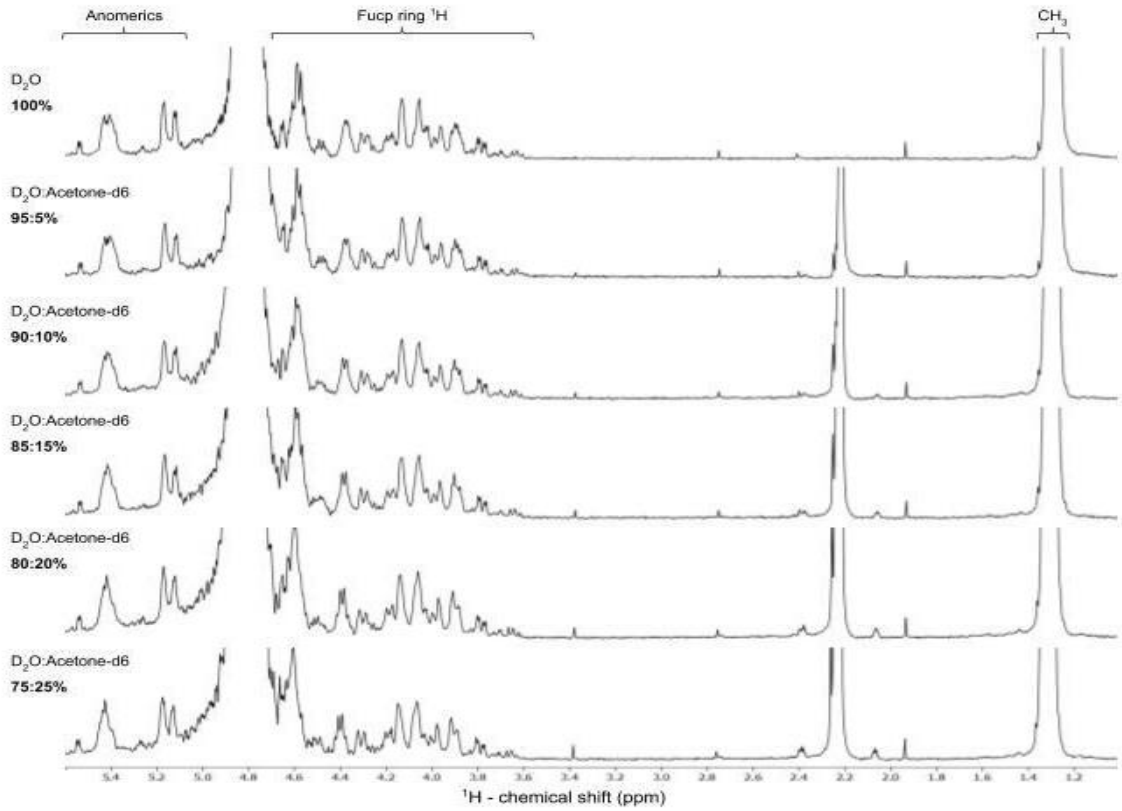

Figure 8: Titration experiment to assess the impact of acetone on the conformation of the sulfated fucan. Each spectrum corresponds to a change of 5% increase in acetone concentration versus deuterium oxide.

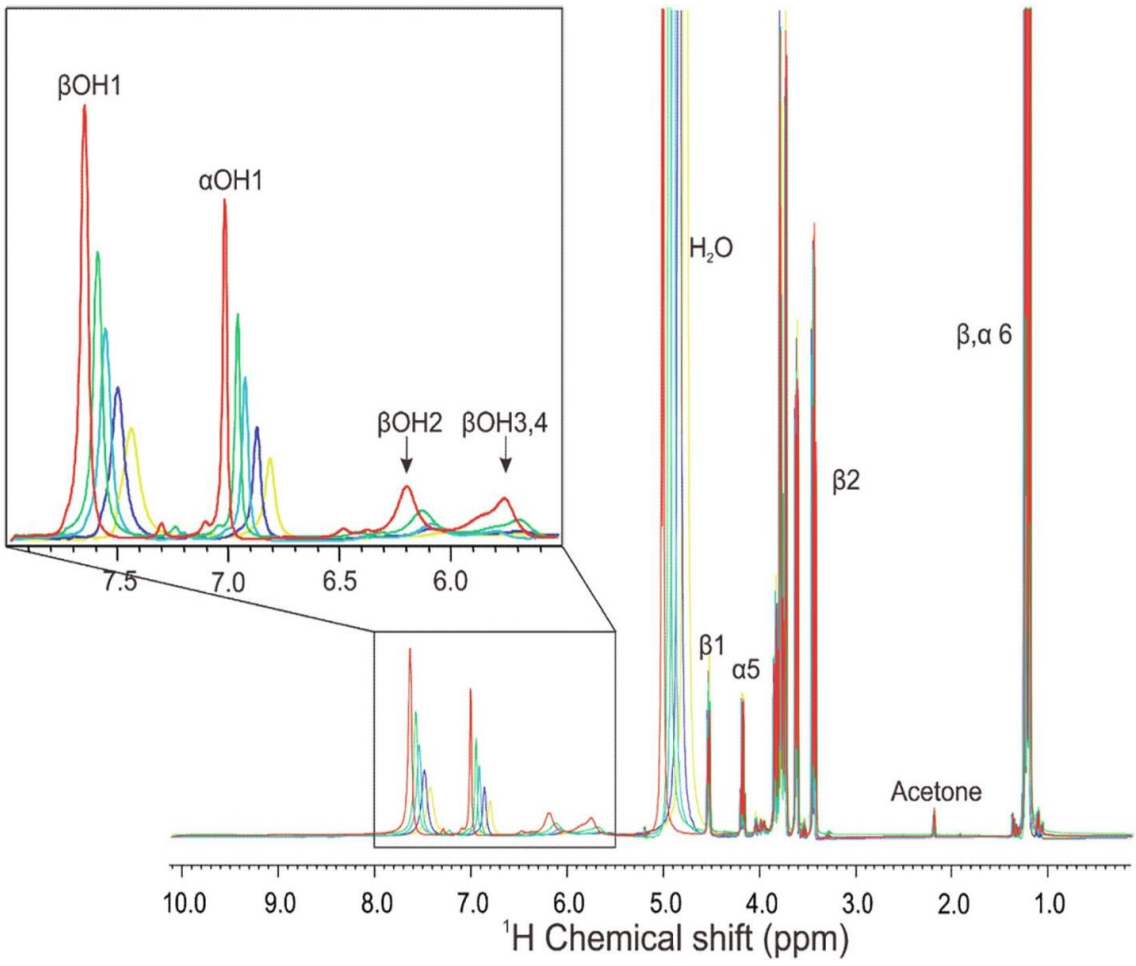

Figure 9: Stacked 1D proton NMR spectra displaying protonation of l-fucose in 85:15 H2O:d6-acetone mixture. Color corresponds to different temperatures the spectrum was acquired at with a stepsize of 5^{o}C.

Temperatures are as follows: Yellow: 25^{o}C, Dark Blue: 20^{o}C, Light Blue: 15^{o}C, Green: 10^{o}C, Red: 5^{o}C

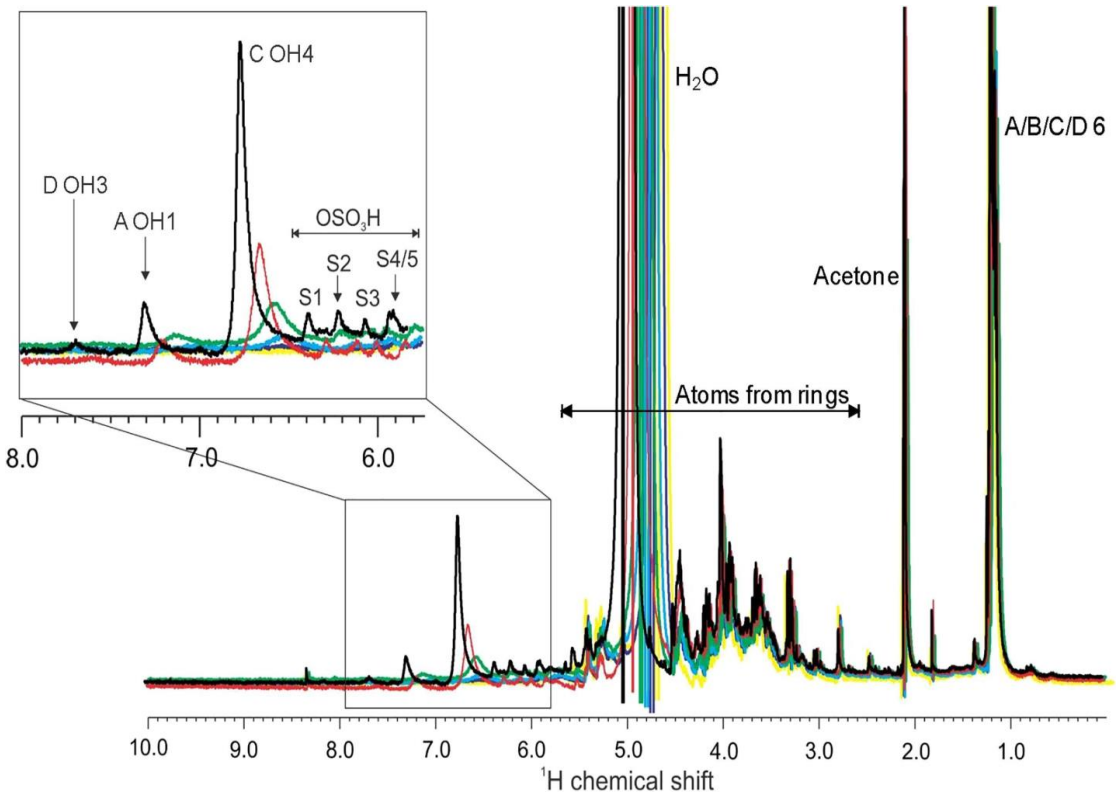

Figure 10: Stacked 1D proton NMR spectra displaying protonation of the sulfated fucan tetramer in 85:15 H_2O:d6-acetone mixture. Color corresponds to different temperatures the spectrum was acquired at with a step size of 5°C.

Temperatures are as follows: Yellow: 25°C, Dark Blue: 20°C, Light Blue: 15°C, Green: 10°C, Red: 5°C, Black: 0°C

Usage of these methods allows for observation of NOE peaks between hydroxyl protons and anomeric protons. As multiple temperatures were used NOE buildup curves were created for both 25^{o}C and 5^{o}C. With a reduction in mixing time of ~10 ms for anomeric protons.

This chemical exchange and subsequent reduction in peak intensity results in issues within the NOE derived restraints by having a negative effect on the peak volume of the NOE derived cross peaks that are used in calculating the distance. We observed an addition of 2-4 angstroms to these distances in initial calculations before any normalization was implemented. This placed these distances outside of any modeled information in both fucose and the sulfated fucan. This issue necessitates calibration of these NOE cross peaks as a function of their occupancy of the protons in hydroxyl groups. Within the literature there are multiple methods to determine the chemical exchange of hydroxyl peaks however these are often within proteins or nucleic acids with little information available in regards to signal intensity in sulfated polysaccharides (76).

Measuring chemical exchange is a difficult process to quantify for these protons that are insensitive within the NMR spectra. These methods are usually based in usage of jump return pulse sequences or using other water suppression schemes (77). Because of the high chemical shift degeneracy that is observed in carbohydrate NMR, the water signal reduces intensity of the anomeric protons that are often falling within this signal oscillating around 4.7 ppm. Due to this possible reduction in anomeric intensity these methods could not be used to calibrate the NOEs. It was determined that a different method would be needed to calibrate these peaks.

The solution we employed as described by Adams et al. uses the formula $1/\tau = 1 / T1, + k$. Where tau (τ) is the decay time constant. This tau value is homogenized across all protons on

the sugar and does not need to be experimentally verified. k is the value that corresponds to chemical exchange, or rate of exchange between the solvent and labile site. Algebraically this equation allows for the calculation of chemical exchange through T1 assuming an arbitrary value for tau. For this portion fucose and the sulfated fucan were studied through T1 inversion recovery for calculation of T1 values to be applied to this formula.

3.2.2 T1 INVERSION RECOVERY AND CALCULATION OF T1 RELAXATION TIMES

The T1 inversion recovery (T1IR) pulse sequence seen in **Figure 11** was used to determine the T1 relaxation property of the hydroxyl protons to calculate and later on calibrate the NOE derived distances that were obtained within the NOESY spectrum. Simply put the T1IR pulse sequence can be described as a series of individual scans consisting of a 180 degree pulse followed by a variable delay time which is then followed by another 90 degree pulse. At almost zero delay time this results in a one dimensional spectrum that is in negative phase. At longer delays times all signals in these spectra will be in the proper phase. This is due to the variable delay time filling enough time to allow for the magnetization of the nuclei to equilibrate with B_0 before the following 90 degree pulse. Following the 90 degree pulse the FID is then allowed to return to equilibrium with the external magnetic field for a repeated number of scans as needed. This relaxation step is represented by D1 within the pulse sequence. 90 degree pulses were optimized through topspin command “pulsecal”.

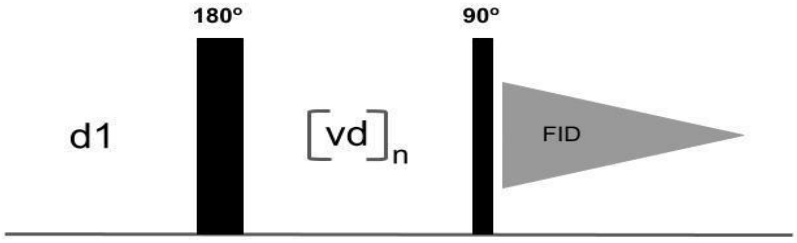

Figure 11: The pulse sequence for T1 inversion recovery is shown. d1 corresponds to standard delay time. Values in degrees correspond to magnetic pulses applied to the sample. $[vd]_n$ corresponds to variable delay times at different values. FID is free induction decay or acquisition.

The T1IR experiment is then conducted out as a sequence of individual 1D protons spectra at differing variable delay times. In the T1 calculation of fucose these times for variable delay were optimized as 0.00125, 0.0025, 0.005, 0.01, 0.01, 0.025, 0.05, 0.1, 0.1, 0.25, 0.5, 0.75, 0.75, 1.25, 3 and 5 sec. In fucose these experiments were performed in protonated spectra at 5°C, 10°C, and 15°C. The result of this acquisition can be observed in **Figure 12.** These vd values were then repeated for the sample containing sulfated fucan. For the sulfated fucan the experiments were ran at 2°C, 5°C, and 8°C. These temperatures were slightly warmer than initial protonation experiments but signals arising were still of quantifiable intensity.

For increasing the validity of the curves derived through the three parameter exponential fit and to have an internal check in the experiment multiple vd values were repeated. Within

these stacked spectra there is a clear pattern of signals being in the negative phase for variable delay times that are near zero and signals either being matched with baseline or being of very low intensity in the spectrum corresponding to a 1.25 second variable delay time. At the following longer delay times the spectra “flip back” to being in the normal phase. This is due to the protons being allowed to relax fully and reach homogeneity with the external magnetic field before the 90 degree pulse followed by acquisition of the FID. In **Figures 13, 14, and 15** experimentally derived curves of values based on vd time value in the x axis as well as relative intensity in the y axis is shown for a representative methyl proton, anomeric proton, and hydroxyl proton. Production of these curves is generated through the following workflow in MestreNova as it is present in the software manual. First, the signal area corresponding to a single proton is selected and plotted in an integrals graph. This results in a table containing vd values in X panel, integral values corresponding with the experimentally acquired signal intensity, then panel Y’(X) the function for three parameter exponential fit [B+F*exp(-x*G)] is selected for plotting. This results in the curves plotted in **Figures 13, 14, and 15** and values corresponding to B, F, and G. T1 value in time is calculated for the inverse of the G value or 1/G = T1. This was repeated for all protons in both the fucose and sulfated tetrasaccharide. An issue highlighted in the original manuscript that due to signal degradation a few protons were unable to have their T1 values calculated from a lack of proper application of the parameter exponential fit function. A majority of protons both carbon-bound and hydroxyl-bound ones were fully described in both MestReNova and TopSpin 4.0.5.

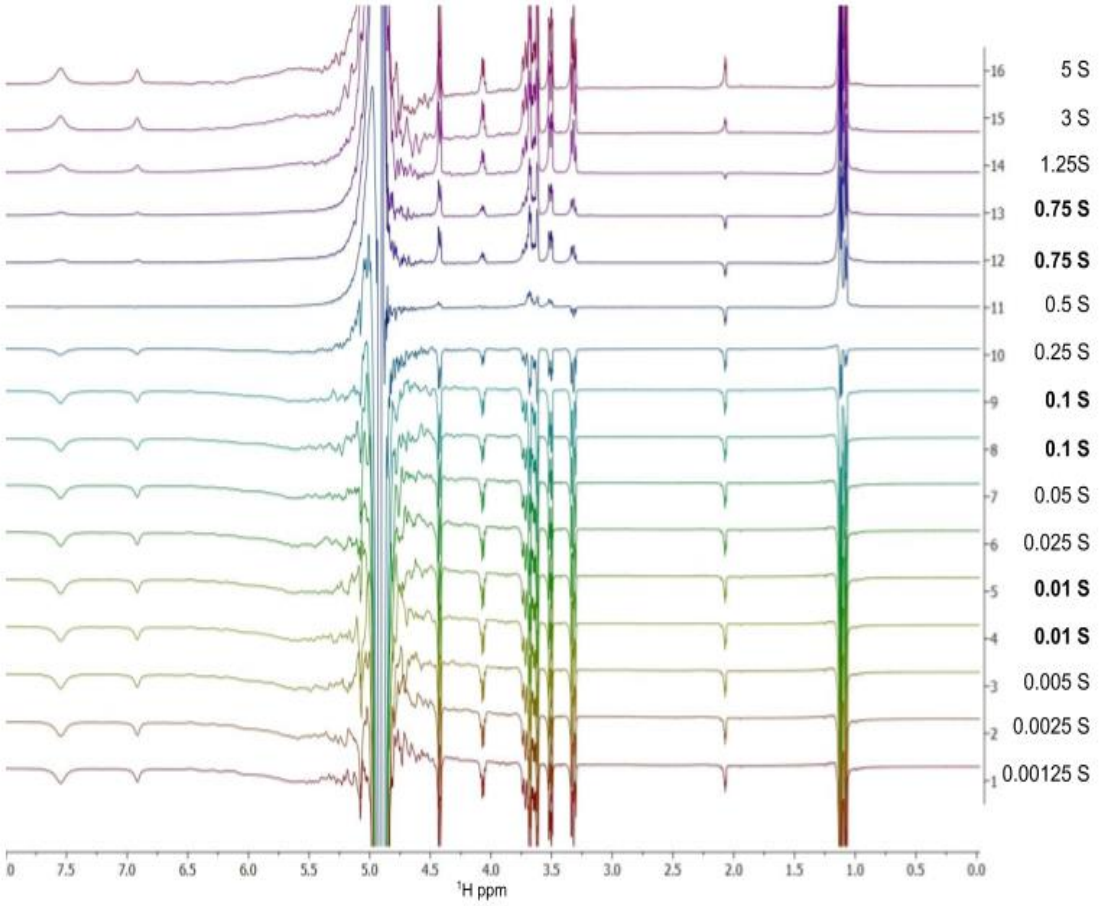

Figure 12: T1 Inversion recovery results of L-fucose in 85:15 H_2O:d6-acetone. X axis corresponds to chemical shift value. Stacked spectra are distinguished by individual vd times. Values highlighted represent repeated vd values.

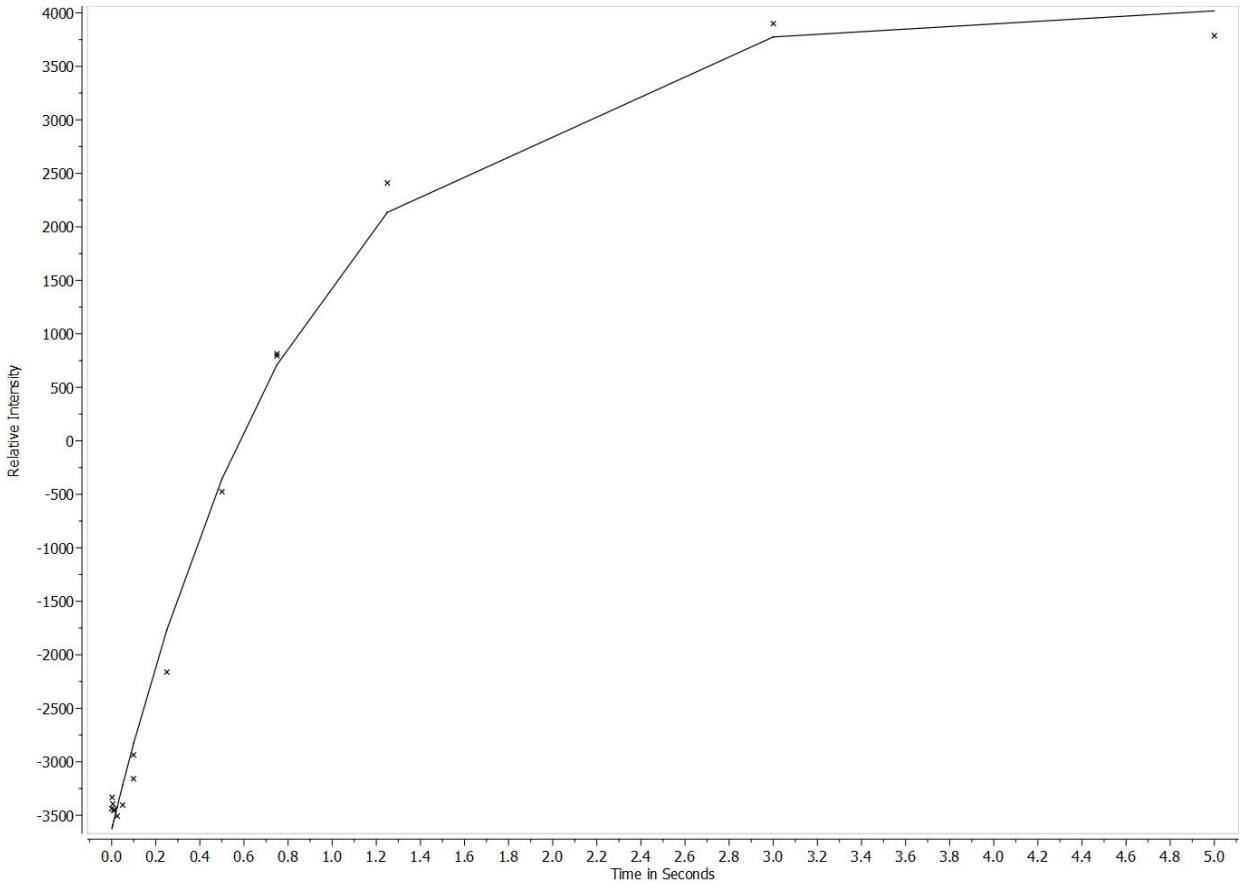

Figure 13: Representative experimentally derived curve for anomeric proton at 3.5 ppm. L-fucose in 85:15 H_2O:d6-acetone. Data was acquired at 15ºC and processed through MNova using a three parameter exponential fit equation (B+F*exp(-x*G)). T1 is then calculated through an inverse of the calculated G value.

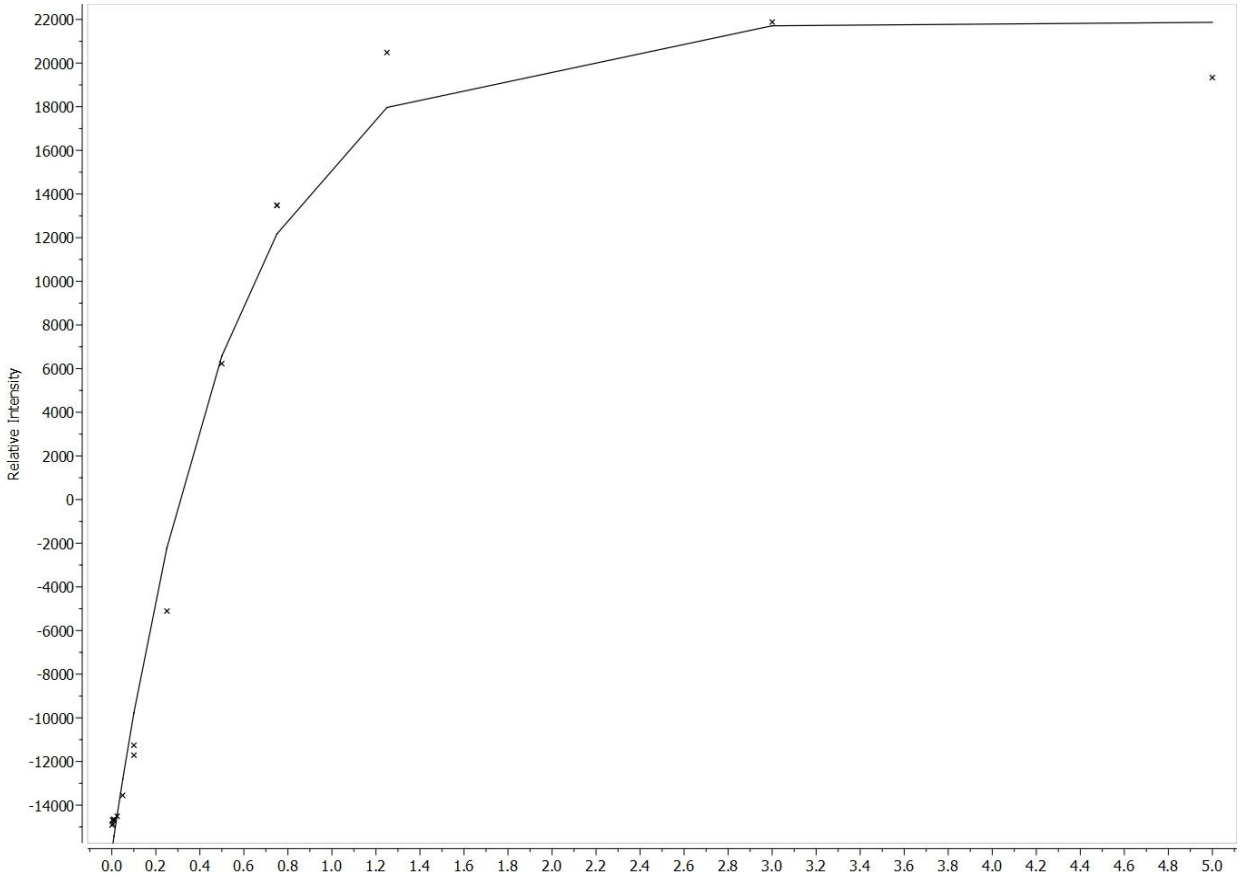

Figure 14: Representative experimentally derived curve for methyl protons at 1.2 ppm. L-fucose in 85:15 H_2O:d6-acetone. Data was acquired at 15^oC and processed through MNova using a three parameter exponential fit equation (B+F*exp(-x*G)). T1 is then calculated through an inverse of the calculated G value.

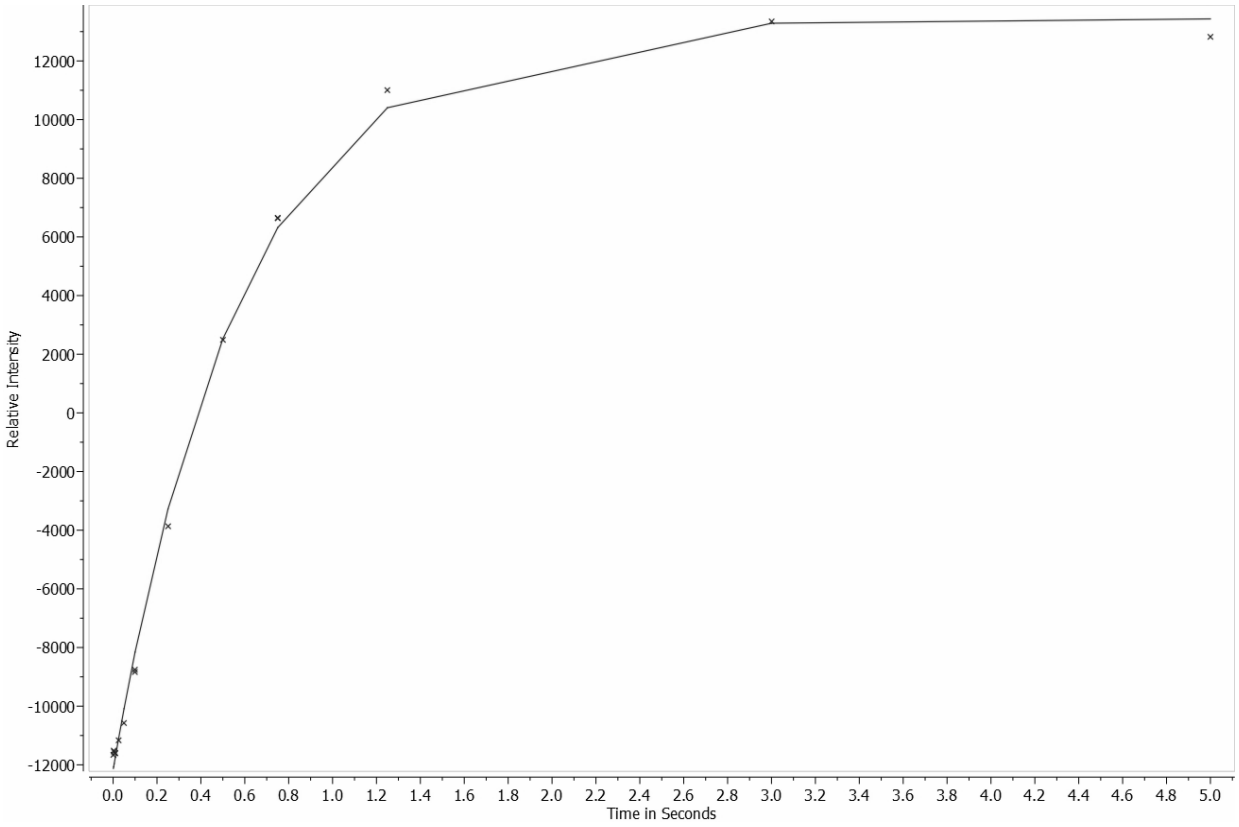

Figure 15: Representative experimentally derived curve for hydroxyl proton at 7 ppm. L-fucose in 85:15 H_2O:d6-acetone. Data was acquired at 15^oC and processed through MNova using a three parameter exponential fit equation (B+F*exp(-x*G)). T1 is then calculated through an inverse of the calculated G value.

3.2.3 EQUILIBRATION OF NOE RESTRAINTS

A compilation of the T1 relaxation times was obtained from integration of the curves for individual peaks. This is presented in **Table 1** for L-fucose. Observation of this information shows a clear pattern of T1 times that are similar within different chemical environments. There are 3 different groups that provide this pattern. These are the protons bound to methyl groups, carbon-bound protons on the fucose backbone, and those that are in the hydroxyl groups. This same pattern is then observed again for the T1 values for the sulfated fucan in **Table 2.**

Table 1: T1IR derived T1 values in L-fucose at 5ºC, 10ºC, and 15ºC with corresponding chemical shift values

1H ppm	Assignment		T1 at 5C	T1 at 10C	T1 at 15C
1.06	α6		0.37s	0.50s	0.55s
1.11	β6		0.42s	0.52s	0.58s
3.33	β2		0.98s	1.53s	1.39s
3.48	β3		0.60s	0.87s	0.90s
3.62	β4		0.63s	0.83s	0.91s
3.67	β5		0.59s	0.77s	0.83s
3.72	α4		0.61s	1.07s	1.06s
3.735	α3		na	na	1.11s
4.05	α5		0.74s	1.23s	1.05s
4.43	β1		0.58s	0.78s	0.86s
	α1		na	na	na
6.9	αOH1		0.65s	0.39s	0.55s
7.52	βOH1		0.65s	0.39s	0.58s
	Full Spectrum		0.69s	0.37s	0.64s

Table 1: T1IR derived T1 values in L-fucose at 5ºC, 10ºC, and 15ºC with corresponding chemical shift values.

Table 2: T1IR derived T1 values in sulfated fucan at 2ºC, 5ºC, and 8ºC with corresponding chemical shift values

1H ppm	Assignment		T1 at 8C	T1 5C	T1 at 2C
1.1	Methyl H		0.31	0.59	0.39
1.2	Methyl H		0.36	0.53	0.36
3.72	D H2		0.84	0.11	0.61
3.82	D H3		0.88	0.1	0.64
4.15	C H3		1.06	0.11	0.67
4.22	A H5		1.18	0.1	0.69
7.18	A OH1		0.47	0.16	0.46
7.7	D OH3		0.5	0.16	0.46

Table 2: T1IR derived T1 values in sulfated fucan at 2ºC, 5ºC, and 8ºC with corresponding chemical shift values. Due to signal degeneration methyl protons experienced almost complete overlap.

Upon comparison between the exchangeable protons T1 values a regular difference was observed for those signals which arise from the hydroxyl protons and those that are carbon-bound in both fucose and the tetrasaccharide. In a simple comparison of means we observed a 40% change in occupancy for fucose and a 35% change in occupancy for the sulfated fucan. The original experimentally observed NOE cross peak derived distance restraints were normalized through these percent changes in occupancy. These interatomic distances are present in **Table 3** for L-fucose and **Tables 4 and 5** for the sulfated fucan.

Table 3: NOE derived interatomic distances for L-fucose in solution

	α-l-Fucp			β-l-Fucp		
NOE	δ 1H–1H (ppm)	1H–1H Distances (Å)		δ 1H–1H (ppm)	1H–1H Distances (Å)	
H1-H2	5.21–3.78	2.4		4.56–3.45	2.9	
H2-H3	3.78–3.86	2.9		3.45–3.64	3	
H3-H4	3.86–3.81	2.5		3.64–3.75	2.6	
H4-H5	3.81–4.20	2.3		na	na	
H5-H6	4.20–1.26	2.5		3.81–1.26	2.3	
OH1-H1	7.00–5.25	2.3		7.63–4.59	2.4	
OH1-H2	7.00–3.76	3.9		7.63–3.50	3.9	
OH2-H2	5.76–3.76	2.9		6.17–3.50	2.3	
OH3-H3	na	na		5.83–3.69	2.3	
OH4-H4	na	na		5.76–3.80	2.3	

Table 3: NOE derived interatomic distances for L-fucose in solution. Information is split between carbon bound protons and exchangeable hydroxyl protons. Exchangeable hydroxyl proton distances are normalized by a 40% change in occupancy relative to chemical exchange.

Table 4. NOE derived interatomic distances for the sulfated fucan tetramer monomer units A and B in solution

	A (reducing 2-sulfated)			B (2,4-disulfated)	
NOE	δ 1H–1H (ppm)	1H–1H Distances (Å)		δ 1H–1H (ppm)	1H–1H Distances (Å)
H1-H2	5.51–4.52	2.4		5.37–4.54	2.4
H2-H3	4.52–4.27	2.6		4.54–4.25	2.7
H3-H4	4.27–4.11	2.4		4.25–4.85	2.6
H5-H6	4.24–1.18	2.5		4.46–1.25	2.9
H1-H3	4.27–5.36	2.6		4.25–5.14	2.4
H1-H4	na	na		na	na
OH1-H1	7.26–5.51	2.1		na	na
OH3-H4	na	na		na	na

Table 4: NOE derived interatomic distances for the sulfated fucan tetramer monomer units A and B in solution. Information is split between carbon-bound protons and exchangeable hydroxyl protons. Exchangeable hydroxyl proton distances are normalized by a 35% change in occupancy relative to chemical exchange.

Table 5: NOE derived interatomic distances for the sulfated fucan tetramer monomer units C and D in solution

	C (2-sulfated)			D (non-reducing 4-sulfated)	
NOE	δ 1H–1H (ppm)	1H–1H Distances (Å)		δ 1H–1H (ppm)	1H–1H Distances (Å)
H1-H2	5.36–4.57	2.5		5.14–3.75	2.4
H2-H3	4.57–4.13	2.8		3.75–4.04	3
H3-H4	na	na		4.04–4.63	2.4
H5-H6	4.11–1.18	2.4		4.55–1.29	2.6
H1-H3	5.36–4.27	2.6		5.14–4.25	2.4
H1-H4	5.36–4.11	2.6		na	na
OH1-H1	na	na		na	na
OH3-H4	na	na		7.62–4.61	3.6

Table 5: NOE derived interatomic distances for the sulfated fucan tetramer monomer units C and D in solution. Information is split between carbon-bound protons and exchangeable hydroxyl protons. Exchangeable hydroxyl proton distances are normalized by a 35% change in occupancy relative to chemical exchange.

In comparison with molecular dynamics data, interatomic distances in fucose were mostly equivalent with force-field derived distances. The force-field used in this structure was GLYCAM06j. This process was repeated for the sulfated fucan. Both simulations matched with great agreement between NMR derived data and force-field information. This is further supported in fucose with atomic distance agreement with a fully sulfated fucose that was described through x-ray crystallography. This fucose was taken from a protein data bank entry, ID: 4CE8. All fucose residues fell into the predicted $^{1}C_{4}$ position.

3.3 CONCLUSIONS

This supports the hypothesis in which it was stated the impact of chemical exchange between solvent protons and hydroxyl residues reduces the NOE peak volume. This method provides a baseline method for normalization of NOE based interatomic distances for fucose and the regular sulfated fucan it has been applied to. In the future applications this method could possibly be applied to other carbohydrate monomers and subsequently more structurally complex carbohydrate polymers like the GAGs. This direction will likely need to be corroborated with regular oligosaccharide structures initially to provide more validation to the methods that have been used. Since there is so little information regarding this area of research, the question must still be asked whether or not differential sulfation patterns and chain length will affect the sugar's conformation in solution in addition to the loss of signal from chemical exchange. In addition to these aspects experimental conditions regarding the isolation and depolymerization of these

oligosaccharides must also be assessed to reduce the possible impact of ionic species on the conformation.

CHAPTER 4. PROTEIN LIGAND INTERACTIONS THROUGH NMR SATURATION TRANSFER DIFFERENCE SPECTROSCOPY

4.1 SATURATION TRANSFER DIFFERENCE (STD)

Multiple methods have been developed in NMR to further understand the complex relationships between ligands and receptors. Among these are chemical shift perturbation experiments that can be used to both map the overall binding locations through differences observed (78). In addition to this NOESY measurements may also be understood to determine the conformation of these proteins in the bound state identifying possible allostery within the peptide (79). These methods however focus on the receptor itself.

Methods have also been developed for understanding the ligand perspective of these interactions. Among these are transferred NOE (trNOE) and saturation transfer difference. trNOE can be conducted to determine the binding conformation of ligands as well as the opportunity to observe the NOE cross-peaks entering negative phase due to the increase of the MW (80). The trNOE method effectively compares the structure of the ligand in the bound vs unbound state. This method does not describe the chemical properties of the ligand that are in interaction however. To understand structurally the nuclei involved within the binding event of these larger complexes saturation transfer difference spectroscopy is the current pinnacle in NMR approaches within this discipline. In "*Saturation Transfer Difference in Characterization*

of Glycosaminoglycan-Protein Interactions" the application of STD to sulfated carbohydrates has been reviewed in detail.

STD is a monumental technique in understanding ligands in interaction with receptors originally described by Meyer and Mayer (34). The strength within this analytical technique from an observation perspective is the ability to observe the protons and functional groups that are in interaction with a receptor. The experiment itself provides a comparison of spectra from the ligand in both the bound and unbound states. This is achieved through a selective magnetization of a receptor of interest with no magnetization of the ligand. Selective magnetization occurs in a region of receptor signals that do not overlap with signals observed in the ligand. This produces a spectrum of signals that are only in interaction with the receptor. Consequently, this allows for a more discrete ability to understand the structure-activity relationship and functional properties of molecules in both drug discovery and pharmacology. In addition to this experiment also allows for the comparison of different ligands within the sample solution, assuming the parameters can be applied for all the ligands of interest. The mechanism for STD is described in **Figure 16.**

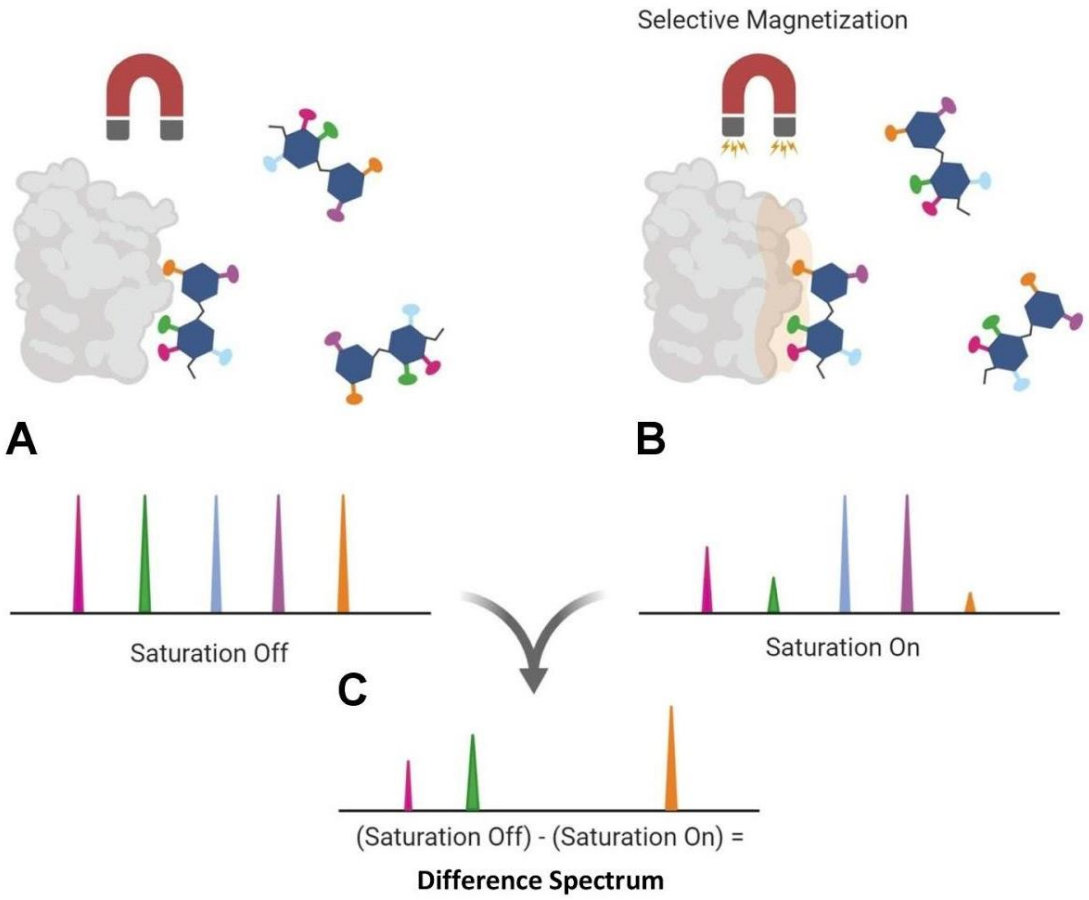

Figure 16: A: Selective saturation to the receptor is off, all signals are observed from the ligand. B: Selective saturation to the receptor is on, ligand signals that are in interaction with the receptor are undergoing cross polarization with shown reduced intensity. C: Difference spectrum is observed between on and off spectra. This leaves only those signals that are involved within the binding mechanism.

STD is conducted through a complex pulse sequence. The beauty of this pulse sequence lies in the selective pulse for magnetization of only the receptor protons. How this is achieved is that this selective pulse irradiates only a region of the spectrum in ppm that corresponds to Larmor frequency of receptor protons. These protons must not fall within the signal range of any of the ligand protons to assure that all signals observed in the spectrum have magnetization that originates through cross polarization from the receptor. This pulse a challenging aspect of the experimental design that must be optimized for proper information to be observed.

In addition to the optimized region in which the spectrum is irradiated the length of this pulse is also a crucial aspect of the experiment. The pulse must be maintained for a long enough period of time for the receptor to be properly magnetized and therefore resulting in highly diffused magnetization throughout the receptor. In another similarity with NOE based experiments the selective saturation pulse is often optimized at different lengths of time to produce a build up curve of intensities (81). When both the length of pulse and design of this saturation step are optimized the receptor will be fully magnetized at the spectra region the pulse has been designed for. Once this has occurred the selectively magnetized region will become diffused across the receptor region. In ligands that are in the bound state this diffusion will further cross polarize through space to the protons in the ligand. This cross polarization event should effectively radiate the ligand protons to the high energy state that is observable through NMR. The cross-polarization that the ligand receives magnetization through is within similar distance restraints to NOE. That is the $1/r^6$ dependence or 5-6 angstroms with intensity reducing greatly as distance between the contacts increases.

Some practical considerations to take into account are the size in MW of the protein as well as other experimental variables like viscosity that need to be considered outside of the pulse design. Due to the property of spin diffusion the magnetization to a specific region of the spectrum is diffused across the biomacromolecule before it migrates through space to the protons bound to the ligand. For this reason this experiment is more effective for larger macromolecules (>15kDa) as this allows for a more intense polarization of interresidues (82)(83). In normal conditions this experiment is conducted by comparison of ligand spectra where both the on and off resonance scans are conducted with a sample containing both ligand and receptor. For the purpose of a control for this experiment to determine no signal is being observed by direct magnetization to the ligand a sample containing only ligand is subjected to the on-resonance frequency. This control experiment to assess the design of the selective pulse assures that the resultant spectrum contains no artifacts due to non-directed pulse to the ligand. When the experiment is performed the receptor and ligand is dissolved within the same sample. To reduce the impact of the protein signals in comparison to the ligand's signals this sample is prepared with a high molar excess of ligand vs. receptor.

In the context of glycobiology saturation transfer difference spectroscopy has been mostly explored into three separate groups biological macromolecules. These are coagulation factors, cytokines and chemokines, and growth factors. While these groups are the most widely probed with this technique there are exceptions. These proteins that have been observed to bind to GAGs are referred to as "heparin binding proteins" or HBPs.

In our manuscript titled "*Saturation Transfer Difference in Characterization of Glycosaminoglycan-Protein Interactions*" the applications of STD towards multiple types of GAGs and these three groups of heparin binding proteins has been explored. It is hypothesized

that the review of this information will lead to conclusions about the impacts of sulfation sites, carbohydrate chain length, and carbohydrate composition and how they vary in these three separate groups of HBPs.

STD application towards GAGs does have an added benefit in application towards GAGs as the selective pulse is often not in overlapping regions of the receptor. This is due to the lack of intense signal overlap as most carbohydrate signals fall within midrange ppm values (84). For this reason the pulse design in these experiments occurred in either high upfield or downfield ppm regions. These ppm regions correspond to methyl groups in the -1 to 1 ppm regions and highly downfield ppm regions corresponding to amine groups present on peptides. These receptor ppm values often correspond to methylene protons in the upfield region and lysine or arginine in the downfield region (85).

As well as experimental design in regards to experimental parameters and conditions differences between structural properties of the GAGs were also well described. In this it was observed that the position of sulfate, sugar monomer composition and oligosaccharide chain length were found to have an impact on STD signals in addition to this the impact of reducing and non-reducing ends was explored in its function towards overall binding of these carbohydrates. Within these three groups a diverse set of structural features was observed to have impact on the STD results. This further exemplified the diversity of the structure-activity relationship of these carbohydrates with a diverse set of protein families. For the purpose of well elucidated interactions between these receptors and the GAGs relatively short oligosaccharide fragments are used to allow for well resolved elucidation of the carbohydrate structures. Tetra-, hexa-, and octasaccharides are often used. Usage of these oligosaccharide chains allows for ease of initial structure elucidation as well as being highly useful for understanding binding

contributions to the regions of the oligosaccharide. The regions within these oligosaccharides are the reducing end, the non-reducing end, and the inner residues. Within STD studies usage of the oligosaccharides provides rich details of these interactions.

While primarily utilized as the more simplistic 1D approach originally described by Meyer and Mayer this is not the only way to perform the STD experiment. More complex ligands or experimental conditions may necessitate usage of alterations of this original pulse sequence. In the case of protein background signals being too overwhelming the usage of saturation transfer double difference (STDD) experiment is used (86). In the STDD experiment the signals from the ligand are not the only signals that are subtracted from the final spectrum as residual signal leftover from the protein in solution is also removed. This assures a final spectrum that is only displaying signals whose origins are from the ligand. In the case where ligand spectrum become too difficult to decipher as they become structurally complex the usage of 2D STD has been implemented. 2D STD experiments that have been successfully used are STD-HSQC and STD-HMQC (87). In an incredibly interesting application of the STD experiment incredibly complementary information to chemical shift perturbation can be observed. That is, where in an inverse of the experiment this transfer of magnetization can be carried out through selective magnetization of the ligand. In an isotopically labeled sample this can be further used to identify those amino acids at the binding interface (88).

4.2 COAGULATION FACTORS

Proteins involved in the coagulation cascade pathway have been the subject for numerous studies regarding GAGs, particularly heparin. This relationship between coagulation and heparin is accentuated by its usage as an anticoagulant since the early 20th century (89). Heparin

contains a pattern of sulfated residues following the pattern GlcNAc/NS(6S)-GlcA-GlcNS(3S,6S)-IdoA(2S)-GlcNS(6S) as seen in **Figure 17**. This pattern has been dubbed fondaparinux in a synthetic preparation and is mimicking the primary binding sequence of heparin to antithrombin. Binding to antithrombin leads to downstream effects in the coagulation cascade and is critical for its physiological function (90). This is primarily observed through inhibition of factors Xa and IIa. Through STD impacts of this pentasaccharide structure were probed in interactions with antithrombin. Stancanelli et al. employed the use of two synthetic hexasaccharides containing this high affinity pentasaccharide sequence. These two structures they had used differed in the composition slightly where one hexasaccharide contains sulfation on the second position of iduronic acid while one does not. This residue was targeted for this change as sulfation on this iduronic acid has long been thought to be a crucial structure in this sequence's biological effects (91). Of note is that this sulfation point was one of two modifications to the pentasaccharide. The other modification was a simple addition of a glucosamine to the reducing end of the pentasaccharide (92). This addition of glucosamine induced no major change to the binding event and produced no notable signals within the STD spectra.

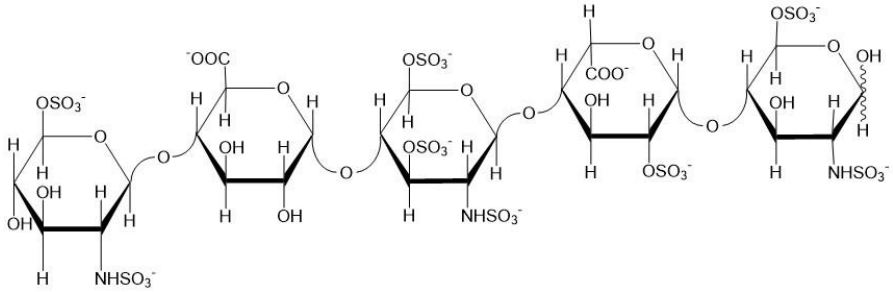

Figure 17: High affinity antithrombin binding HS pentasaccharide structure. [→4)-D-GlcNAc/GlcNS6S-α-(1→4)-D-GlcA-β-(1→4)-D-GlcNS3S6S-α-(1→4)-L-IdoA2S-α-(1→4)-D-GlcNS6S-α-(1→]

Through STD between these hexasaccharides and antithrombin the individual contributions of structural features are described. The intensity of these interactions is visually available by **Figure 18.** Conclusions from this STD study concluded that the contribution of sulfation on the second position of iduronic acid is not a requirement for this pentasaccharides binding to antithrombin.

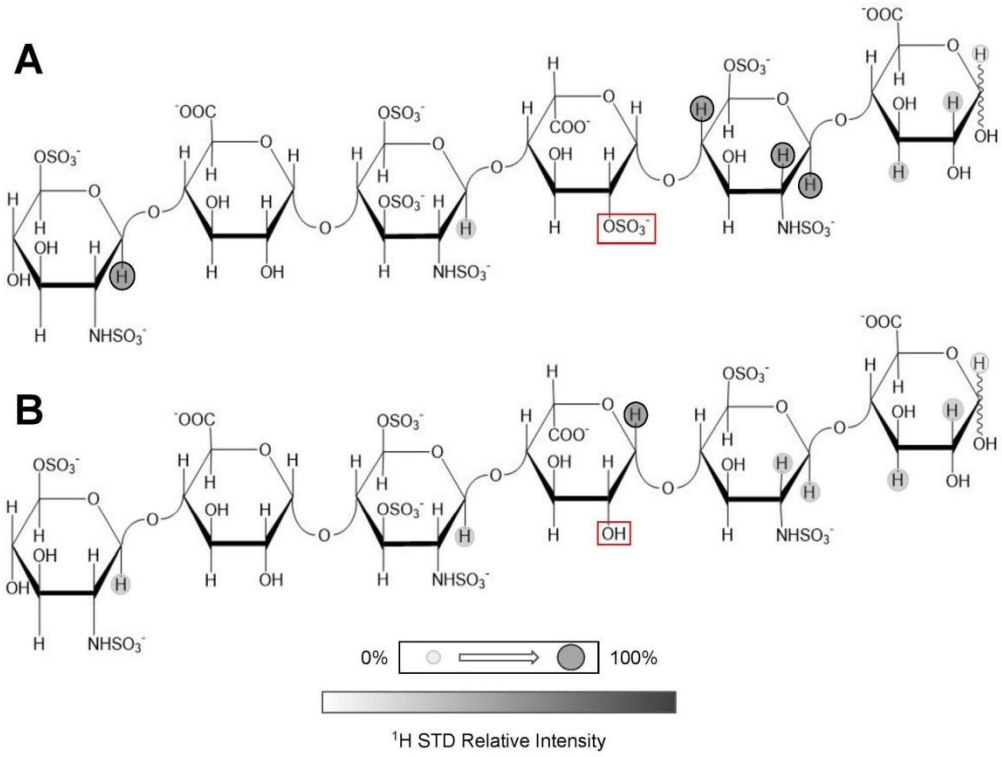

Figure 18: Hexasaccharides containing high affinity AT-binding sequence used in STD studies with antithrombin. Both differ slightly in sulfation content as is highlighted by red boxes at differing residues. A: Contains sulfation on the second position of iduronic acid. B: Does not contain sulfation at the second position of iduronic acid. Grey markers correspond to the STD derived signal intensities. Signal intensity markers are relative to the maximum observed proton intensity in the STD NMR spectrum for each individual ligand.

The structural properties of this pentasaccharide structure were further explored by Guerrini et al. who elucidated the importance of 3-O sulfation on GlcNS(6S) within this pentasaccharide structure (93). This alteration resulted in an oligosaccharide with 3-O sulfation on two monosaccharide units. For this they opted for usage of a longer oligosaccharide fragment, an octamer in this case. With the presence of this additional 3-O sulfate group they observed a clear increase in STD intensity. This further provided evidence for the importance of sulfation on this position of GlcN.

Through these two studies the usage of saturation transfer difference was able to discern and somewhat quantify the impact of structural features of this pentasaccharide with antithrombin, particularly the IdoA2S motif. It was observed that increases to the oligosaccharide chain did not heavily impact the interaction between antithrombin and GlcNAc/NS(6S)-GlcA-GlcNS(3S,6S)-IdoA(2S)-GlcNS(6S). It is also observed that the impact of sulfation on IdoA is not of maximum importance while further highlighting the importance of 3-O sulfation.

4.3 CYTOKINES AND CHEMOKINES

Cytokines and chemokines are likely the most well explored HBPs through STD NMR. In this review many of these macromolecules in this category were described through STD. Of these are GBP Stromal Cell-derived Factor-1 alpha (CXCL12α), Midkine (MK), C-C Motif Chemokine Ligand 5 (CCL5), Interleukin-10 (IL-10), and Leukocyte common antigen-related (LAR). Within these different cytokines and chemokines many structural conclusions about GAGs could be made. This is due to the sheer abundance of structural diversity of receptor molecules that was able to be observed in this group of HBPs.

One of these proteins, GBP stromal cell-derived factor-1 alpha (CXCL12α), is expressed throughout multiple cell types (94). Coupled with this proteins known binding capacity for heparin, this highlights the importance of glycosaminoglycans as cellular components (95). In application towards CXCL12α Laguri et. al (96) utilized a fully synthetic heparin octasaccharide for their STD studies. In this case synthesis of this allowed for isotopic labelling of carbon residues in the oligosaccharide. When applied in the STD experiment a similar pattern of intensity was seen as observed in Fei Yu's work in the growth factors. This is observed in **Figure 19.** Through observation of the signal intensities it is apparent that this molecular complex is formed through bonding within the center disaccharides with little or low influence from the reducing and non-reducing ends (96).

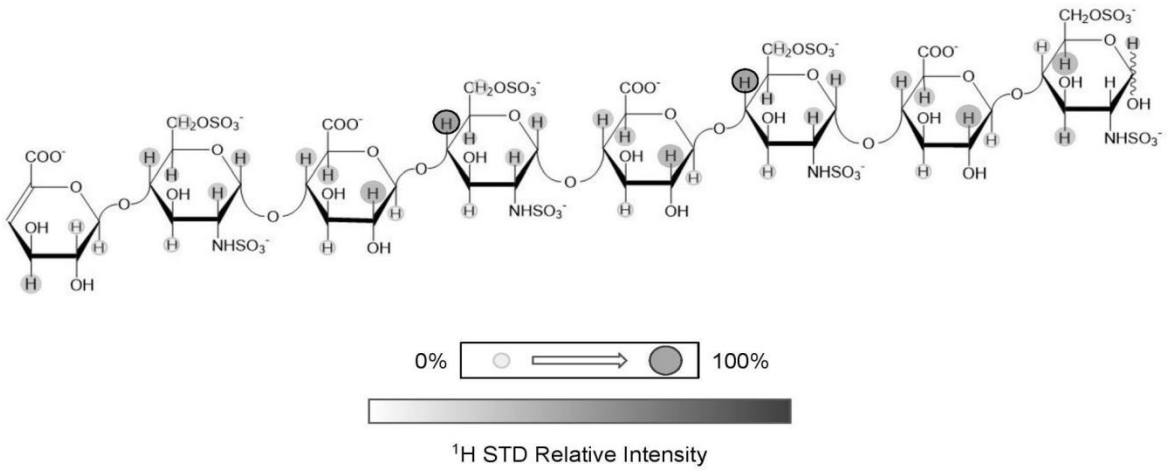

Figure 19: HS octasaccharide is displayed. This oligosaccharide contains the GlcNS6S residue. STD derived signal intensities are displayed by the gray markers present. Signal intensity markers are relative to the maximum observed proton intensity in the STD NMR spectrum.

In interaction with midkine, the impact of GAGs is also described well within the literature with physiological impacts being quite widespread (97). For STD studies regarding this protein Solera et al. opted to use two chondroitin sulfate oligosaccharides (98). These CS oligosaccharides consisted of 4 monomer units with structures being described as follows, GalNAc4S6S-GlcA3S-GalNAc4S6S-GlcA3S and IdoA2S4S-GalNAc4S6S-IdoA2S4S-GalNAc4S6S. These tetrasaccharides differ in both sulfation content and sugar constituents. When applied in STD both sugars were found to sequester magnetization across the entirety of the chain. This indicated that the binding event and subsequent complex involved the entirety of the oligosaccharide without an intense impact from their differences in structural constituents. In **Figure 20** these intensities are displayed. In comparison to other STD effects in different GAG:Protein complexes these showed a preference for the reducing ends in both oligosaccharides. The second oligosaccharide shows increased intensities on innermost residues. While not entirely clear this may be due to the hinge action that occurs during bound conformation of this molecule (99). This hinge action within this protein has been observed within midkine itself (88) however this is the first time this function could be observed through the ligand's perspective.

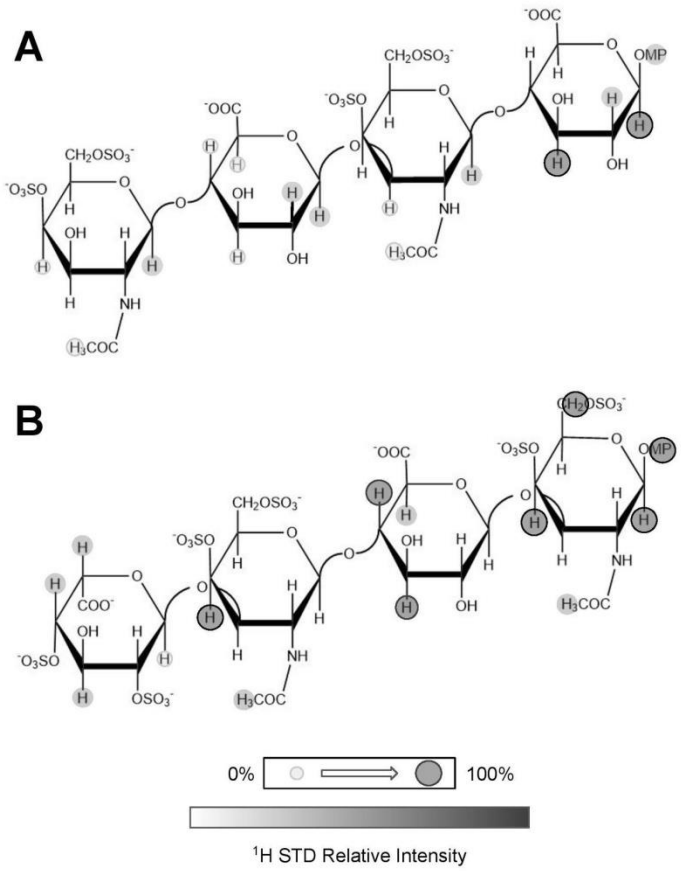

Figure 20: CS tetrasaccharides used in STD studies with midkine. A: contains a GalNAc4S6S residue. B: contains an iduronic acid as opposed to a glucuronic acid. This residue is 2,4 sulfated. Gray markers indicated experimentally derived STD signal intensities. Signal intensity markers are relative to the maximum observed proton intensity in the STD NMR spectrum for each individual ligand.

CCL5 is another immunoregulatory protein where it functions in inflammation to promote cell migrations (100). It has been observed that CCL5 has a mechanism that requires it to be in complex with a GAG to exert its biological effects (101). Because of this requirement of GAGs in its function CCL5 serves as an excellent receptor for discerning structural features

required for its GAG interaction. For this application Deshauer et al. sought to use chondroitin sulfate hexasaccharides to probe the structural influence of GAGs with CCL5 (102). These chondroitin sulfates differed in sulfate position in the disaccharide building blocks. Within this study it was concluded that the binding interface is in interaction with the entirety of the oligosaccharide chain and not solely from those residues that are sulfated. In an interesting application Deshauer's group also utilized the inverse of this STD experiment, 2D HSQC STD NMR, to obtain the amino acid residues also involved in this binding. This is both in inverse in results but also an inverse in preparation where the receptor is in molar excess in comparison the ligand. This provides more support to previously obtained NMR based information about the amino acid residues involved in this binding event (88).

In application towards another anti-inflammatory cytokine, Interleukin-10 (IL-10), Kunze et al. applied the usage of multiple glycosaminoglycans types. These were CS, DS, HA, and heparin (103). In their studies they found a similar pattern as many other STD studies of GAGs in which the protons nearing sulfate groups were the most heavily involved within the binding interface during the formation of the Protein:Ligand complex. This was performed in both 1D STD NMR and 2D HSQC NMR. Upon removal of sulfate groups this interaction was even clearer where a reduction in STD signal intensity was observed for the same protons involved. This was in contrast to an experiment in which they observed a tighter binding event in a tri-sulfated CS residue versus a di-sulfated CS residue. To probe a different structural feature observed in carbohydrate polymers, the length of the oligosaccharide chain itself, Kunze et al. also performed these STD experiments with heparin oligosaccharides of differing lengths from a disaccharide to a decasaccharide. It was observed that the longer the oligosaccharide chain the

more intense the interaction occurred as notified through the signal intensities and lower concentration requirement.

Another chemokine, leukocyte common antigen-related (LAR), was explored through STD. Of note is that this chemokine is not directly involved in the inflammatory processes as some of the other proteins that have been discussed. LAR is heavily involved in axon growth and elongation where heparan containing proteoglycans promote proliferation of the physiological outcomes while chondroitin sulfates promotes the opposite (104)(105)(106). For STD studies the pentasaccharide sequence with high affinity for antithrombin, GlcNAc/NS(6S)-GlcA-GlcNS(3S,6S)-IdoA(2S)-GlcNS(6S), was used by Gao et al. (107). In these experiments the usage of STDD experiments were used to reduce the amount of background noise from the peptide within the solution. Conclusions acquired from this pentasaccharide sequence with LAR yielded a pattern of signals corresponding to protons in the non-reducing end of this oligosaccharide. This was concluded as being the result of less sulfation on this end of the sugar, further highlighting the structural diversity of GAGs in regards to physiological outcomes and binding partners.

4.4 GROWTH FACTORS

Interactions between growth factors and GAGs are a well described relationship with multiple growth factor families having been shown to be in interaction with GAGs (108). This relationship is especially well described within fibroblast growth factors, a family of growth factors consisting of 23 members sharing a conserved peptide sequence (109).While this relationship is diverse in families of growth factors, those studied through STD are much more limited with these experiments only being performed for fibroblast growth factors at this time.

This work was conducted by Fei Yu et. al (85) and produced excellent conclusions in regards to structural diversity's impact upon binding.

In these studies Fei Yu utilized three synthetic heparin octasaccharides. These oligosaccharides differed by sulfation sites with no alterations in their monosaccharide constituents. Within these each oligosaccharide is composed of disulfated disaccharides with only one of the three containing a disulfated monomer unit. With these octasaccharides STD was performed with two members of the FGF super-family, FGF-2 and FGF-10. Between these two FGFs there was clear differences observed within the STD spectra. Namely, that FGF-2 has a binding capacity much more indicative of a specific structural requirement. This was highlighted by signals within the STD only showing discrete increases in intensity of 2 out of 3 oligosaccharides. In this case octasaccharide 3 was the only sugar displayed well resolved peaks indicative of exact structural moieties involved in the binding. This was further supported through the usage of all three oligosaccharides within the same sample. In this combinatorial experiment it was observed that the signals present in the STD spectrum were from oligosaccharide 3. Possibly indicating that due to a more preferential structure to FGF-2 that this oligosaccharide out competed the other two within the same solution. This is apparent in **Figure 21** where this interaction is shown through this enhanced signal intensities. Within FGF-10 this pattern is not seen and no oligosaccharide displays a clear preferential binding structure. This is in stark contrast to FGF-2 interactions that did show this specificity.

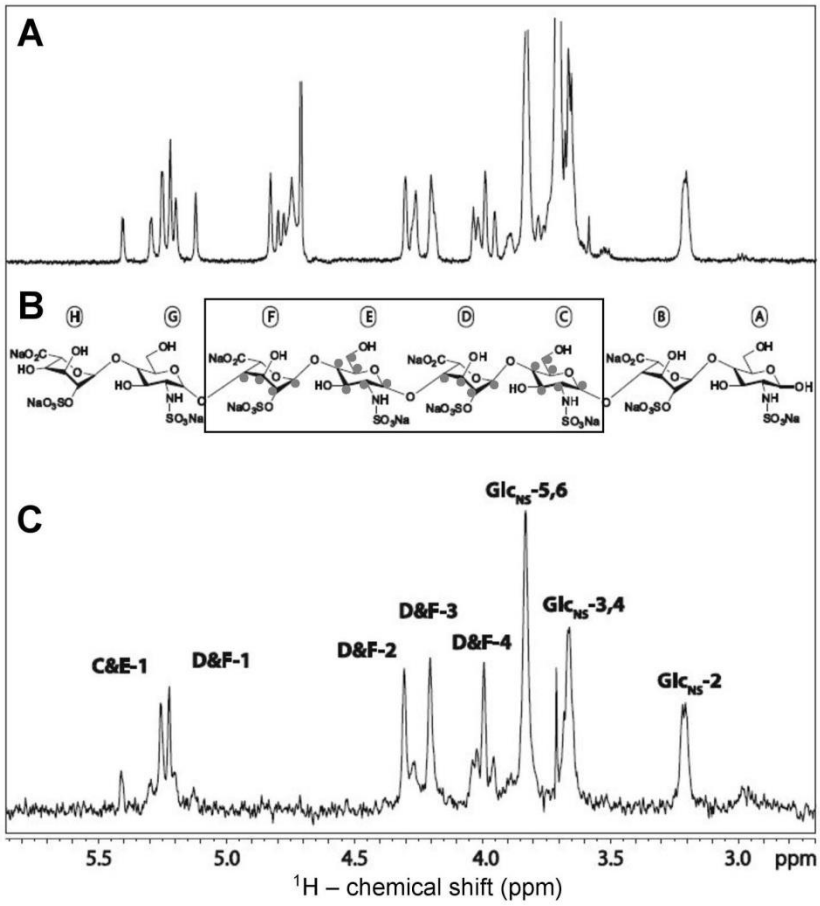

Figure 21: STD information as related to Hp octasaccharide in interaction with FGF-2. A: Reference 1D NMR spectrum Hp octasaccharide. B: Structure of the Hp octasaccharide, individual monomer constituents are labelled accordingly. Boxed in area represents the region of the highest affinity for FGF-2. C: STD spectrum of the Hp octasaccharide, gray dots in (B) correspond to these signals.

Of importance to note in these experiments is the lack of signal arising from both reducing and non-reducing ends of the oligosaccharides. This indicates that the binding is primarily a function of the innermost disaccharide units with the receptors.

4.5 CONCLUSIONS

Currently, it is very clear that the impact of sulfation pattern, chain length, and monosaccharide content are distinct parameters involved in the binding capacities of these carbohydrates as was hypothesized. This is highlighted by the diversity in results observed in STD studies involved GAGs and their already known binding partners. STD has allowed for the determination of structural importance of the location of sulfation in these carbohydrates. This is highlighted through experiments involving complex mixtures of similar oligosaccharides, STD signal intensities as a result of presence of lack of sulfation at specific residues. These conclusions regarding the diversity of glycosaminoglycans will aid future research identifying the epitopes and structural motifs required for GAG binding. This will allow for both further understanding of the mechanisms of these interactions as well as more supported routes of development for pharmaceutical candidates.

REFERENCE LIST

1. Becker, E. D. (1993). A BRIEF HISTORY OF NUCLEAR MAGNETIC RESONANCE. Analytical Chemistry, 65(6), 295A–302A. https://doi.org/10.1021/ac00054a716

2. Fiaux, J., Bertelsen, E. B., Horwich, A. L., & Wüthrich, K. (2002). NMR analysis of a 900K GroEL–GroES complex. Nature, 418(6894), 207–211. https://doi.org/10.1038/nature00860

3. McConnell, H. M. (1958). Reaction Rates by Nuclear Magnetic Resonance. The Journal of Chemical Physics, 28(3), 430–431. https://doi.org/10.1063/1.1744152

4. Wishart, D. S. (2008). Quantitative metabolomics using NMR. TrAC Trends in Analytical Chemistry, 27(3), 228–237. https://doi.org/10.1016/j.trac.2007.12.001

5. Clark-Lewis, I., Kim, K.-S., Rajarathnam, K., Gong, J.-H., Dewald, B., Moser, B., Baggiolini, M., & Sykes, B. D. (1995). Structure-activity relationships of chemokines. Journal of Leukocyte Biology, 57(5), 703–711. https://doi.org/10.1002/jlb.57.5.703

6. Lane, A. N., & Arumugam, S. (2005). Improving NMR sensitivity in room temperature and cooled probes with dipolar ions. Journal of Magnetic Resonance, 173(2), 339–343. https://doi.org/10.1016/j.jmr.2005.01.005

7. Spiess, H. W. (1991). Structure and dynamics of solid polymers from 2D- and 3D-NMR. Chemical Reviews, 91(7), 1321–1338. https://doi.org/10.1021/cr00007a002

8. Bax, A., & Grzesiek, S. (1993). Methodological advances in protein NMR. Accounts of Chemical Research, 26(4), 131–138. https://doi.org/10.1021/ar00028a001

9. Gorenstein, D. G. (1992). [14] 31P NMR of DNA. In DNA Structures Part A: Synthesis and Physical Analysis of DNA (pp. 254–286). Elsevier. https://doi.org/10.1016/0076-6879(92)11016-c

10. Kupferschmitt, G., Schmidt, J., Schmidt, T., Fera, B., Buck, F., & Riiterjans, H. (1987). 15N labeling of oligodeoxynucleotides for NMR studies of DNA-ligand interactions. Nucleic Acids Research, 15(15), 6225–6241. https://doi.org/10.1093/nar/15.15.6225

11. Meyer, B., & Peters, T. (2003). NMR Spectroscopy Techniques for Screening and Identifying Ligand Binding to Protein Receptors. Angewandte Chemie International Edition, 42(8), 864–890. https://doi.org/10.1002/anie.200390233

12. Clore, G. M., & Gronenborn, A. M. (2009). Structures of Larger Proteins, Protein-Ligand, and Protein-DNA Complexes by Multidimensional Heteronuclear NMR. In Encyclopedia of Magnetic Resonance. John Wiley & Sons, Ltd. https://doi.org/10.1002/9780470034590.emrstm0542.pub2

13. Cordier, F., & Grzesiek, S. (2002). Temperature-dependence of protein hydrogen bond properties as studied by high-resolution NMR 1 1Edited by P. E. Wright. Journal of Molecular Biology, 317(5), 739–752. https://doi.org/10.1006/jmbi.2002.5446

14. Zhang, Y.-Z., Roder, H., & Paterson, Y. (2008). Rapid amide proton exchange rates in peptides and proteins measured by solvent quenching and two-dimensional NMR. Protein Science, 4(4), 804–814. https://doi.org/10.1002/pro.5560040420

15. Ishihara, Y., Calderon, A., Watanabe, H., Okamoto, K., Suzuki, Y., Kuroda, K., & Suzuki, Y. (1995). A precise and fast temperature mapping using water proton chemical shift. Magnetic Resonance in Medicine, 34(6), 814–823. https://doi.org/10.1002/mrm.1910340606

16. Jameson, C. J., Jameson, A. K., & Cohen, S. M. (1973). Temperature and density dependence of 129Xe chemical shift in xenon gas. The Journal of Chemical Physics, 59(8), 4540–4546. https://doi.org/10.1063/1.1680652

17. Cornilescu, G., Marquardt, J. L., Ottiger, M., & Bax, A. (1998). Validation of Protein Structure from Anisotropic Carbonyl Chemical Shifts in a Dilute Liquid Crystalline Phase. Journal of the American Chemical Society, 120(27), 6836–6837. https://doi.org/10.1021/ja9812610

18. Schleich, T., Blackburn, B. J., Lapper, R. D., & Smith, I. C. P. (1972). Nuclear magnetic resonance study of the influence of aqueous sodium perchlorate and temperature on the solution confromations of uracil nucleosides and nucleotides. Biochemistry, 11(2), 137–145. https://doi.org/10.1021/bi00752a001

19. de Dios, A. C., & Jameson, C. J. (1994). The NMR Chemical Shift: Insight into Structure and Environment. In Annual Reports on NMR Spectroscopy (pp. 1–69). Elsevier. https://doi.org/10.1016/s0066-4103(08)60130-1

20. Ehnbom, A., Hall, M. B., & Gladysz, J. A. (2019). Origin of Shielding and Deshielding Effects in NMR Spectra of Organic Conjugated Polyynes. Organic Letters, 21(3), 753–757. https://doi.org/10.1021/acs.orglett.8b03990

21. Schumann, F. H., Riepl, H., Maurer, T., Gronwald, W., Neidig, K.-P., & Kalbitzer, H. R. (2007). Combined chemical shift changes and amino acid specific chemical shift mapping of protein–protein interactions. Journal of Biomolecular NMR, 39(4), 275–289. https://doi.org/10.1007/s10858-007-9197-z

22. M. A. WENDT J. MEILER F. WEINHOLD T. (1998). Solvent and concentration dependence of the hydroxyl chemical shift of methanol. Molecular Physics, 93(1), 145–152. https://doi.org/10.1080/002689798169537

23. Li, H., Yamada, H., & Akasaka, K. (1998). Effect of Pressure on Individual Hydrogen Bonds in Proteins. Basic Pancreatic Trypsin Inhibitor†. Biochemistry, 37(5), 1167–1173. https://doi.org/10.1021/bi972288j

24. Lerner, D. B., & Kearns, D. R. (1980). Observation of large solvent effects on the phosphorus-31 NMR chemical shifts of nucleotides. Journal of the American Chemical Society, 102(25), 7611–7612. https://doi.org/10.1021/ja00545a059

25. Barone, V., Peralta, J. E., Contreras, R. H., Sosnin, A. V., & Krivdin, L. B. (2001). NaturalJ coupling (NJC) analysis of the electron lone pair effect on NMR couplings: Part 1. The lone pair orientation effect of an ?-nitrogen atom on1J(C,C) couplings. Magnetic Resonance in Chemistry, 39(10), 600–606. https://doi.org/10.1002/mrc.901

26. Dingley, A. J., Cordier, F., & Grzesiek, S. (2001). An introduction to hydrogen bond scalar couplings. Concepts in Magnetic Resonance, 13(2), 103–127. https://doi.org/10.1002/1099-0534(2001)13:2<103::aid-cmr1001>3.0.co;2-m

27. Govindaraju, V., Young, K., & Maudsley, A. A. (2000). Proton NMR chemical shifts and coupling constants for brain metabolites. NMR in Biomedicine, 13(3), 129–153. https://doi.org/10.1002/1099-1492(200005)13:3<129::aid-nbm619>3.0.co;2-v

28. Kingsley, P. B. (1999). Methods of measuring spin-lattice (T1) relaxation times: An annotated bibliography. Concepts in Magnetic Resonance, 11(4), 243–276. https://doi.org/10.1002/(sici)1099-0534(1999)11:4<243::aid-cmr5>3.0.co;2-c

29. Haslinger, E., & Lynden-Bell, R. . (1978). Investigation of the internal rotation of methyl groups by T1 relaxation measurements. Journal of Magnetic Resonance (1969), 31(1), 33–40. https://doi.org/10.1016/0022-2364(78)90166-

30. Pastor, R. W., Venable, R. M., Karplus, M., & Szabo, A. (1988). A simulation based model of NMRT1relaxation in lipid bilayer vesicles. The Journal of Chemical Physics, 89(2), 1128–1140. https://doi.org/10.1063/1.455219

31. Chen, J., Chang, E. Y., Carl, M., Ma, Y., Shao, H., Chen, B., Wu, Z., & Du, J. (2016). Measurement of bound and pore water T1 relaxation times in cortical bone using three-dimensional ultrashort echo time cones sequences. Magnetic Resonance in Medicine, 77(6), 2136–2145. https://doi.org/10.1002/mrm.26292

32. Thomsen, C., Sørensen, P. G., Karle, H., Christoffersen, P., & Henriksen, O. (1987). Prolonged bone marrow T1-relaxation in acute leukaemia. In vivo tissue characterization by magnetic resonance imaging. Magnetic Resonance Imaging, 5(4), 251–257. https://doi.org/10.1016/0730-725x(87)90001-4

33. Katsube, T., Okada, M., Kumano, S., Hori, M., Imaoka, I., Ishii, K., Kudo, M., Kitagaki, H., & Murakami, T. (2011). Estimation of Liver Function Using T1 Mapping on Gd-EOB-DTPA-Enhanced Magnetic Resonance Imaging. Investigative Radiology, 46(4), 277–283. https://doi.org/10.1097/rli.0b013e318200f67d

34. Mayer, M., & Meyer, B. (1999). Characterization of Ligand Binding by Saturation Transfer Difference NMR Spectroscopy. Angewandte Chemie International Edition, 38(12), 1784–1788. https://doi.org/10.1002/(sici)1521-3773(19990614)38:12<1784::aid-anie1784>3.0.co;2-q

35. Kay, L., Keifer, P., & Saarinen, T. (1992). Pure absorption gradient enhanced heteronuclear single quantum correlation spectroscopy with improved sensitivity. Journal of the American Chemical Society, 114(26), 10663–10665. https://doi.org/10.1021/ja00052a088

36. Dwek, R. A. (1996). Glycobiology: Toward Understanding the Function of Sugars. Chemical Reviews, 96(2), 683–720. https://doi.org/10.1021/cr940283b
37. Hart, G. W., & Copeland, R. J. (2010). Glycomics Hits the Big Time. Cell, 143(5), 672–676. https://doi.org/10.1016/j.cell.2010.11.008

38. Latgé, J. (2007). The cell wall: a carbohydrate armour for the fungal cell. Molecular Microbiology, 66(2), 279–290. https://doi.org/10.1111/j.1365-2958.2007.05872.x

39. Hoiczyk, E., & Hansel, A. (2000). Cyanobacterial Cell Walls: News from an Unusual Prokaryotic Envelope. Journal of Bacteriology, 182(5), 1191–1199. https://doi.org/10.1128/jb.182.5.1191-1199.2000

40. Dityatev, A., & Schachner, M. (2003). Extracellular matrix molecules and synaptic plasticity. Nature Reviews Neuroscience, 4(6), 456–468. https://doi.org/10.1038/nrn1115

41. Pomin, V. H. (2015). Sulfated glycans in inflammation. European Journal of Medicinal Chemistry, 92, 353–369. https://doi.org/10.1016/j.ejmech.2015.01.002

42. Ghatak, S., Maytin, E. V., Mack, J. A., Hascall, V. C., Atanelishvili, I., Moreno Rodriguez, R., Markwald, R. R., & Misra, S. (2015). Roles of Proteoglycans and Glycosaminoglycans in Wound Healing and Fibrosis. International Journal of Cell Biology, 2015, 1–20. https://doi.org/10.1155/2015/834893

43. Yip, G. W. (2006). Therapeutic value of glycosaminoglycans in cancer. Molecular Cancer Therapeutics, 5(9), 2139–2148. https://doi.org/10.1158/1535-7163.mct-06-0082

44. Hayes, A. J., & Melrose, J. (2018). Glycans and glycosaminoglycans in neurobiology: key regulators of neuronal cell function and fate. Biochemical Journal, 475(15), 2511–2545. https://doi.org/10.1042/bcj20180283

45. Kaiser, P., Harenberg, J., Walenga, J. M., Huhle, G., Giese, C., Prechel, M., Hoppensteadt, D., & Fareed, J. (2001). Effects of a Heparin-Binding Protein on Blood Coagulation and Platelet Function. Seminars in Thrombosis and Hemostasis, 27(5), 495–502. https://doi.org/10.1055/s-2001-17960

46. Pomin, V., & Mulloy, B. (2018). Glycosaminoglycans and Proteoglycans. Pharmaceuticals, 11(1), 27. https://doi.org/10.3390/ph11010027

47. Funderburgh, J. L. (2000). MINI REVIEW Keratan sulfate: structure, biosynthesis, and function. Glycobiology, 10(10), 951–958. https://doi.org/10.1093/glycob/10.10.951

48. Balazs, E. A., Watson, D., Duff, I. F., & Roseman, S. (1967). Hyaluronic acid in synovial fluid. I. Molecular parameters of hyaluronic acid in normal and arthritic human fluids. Arthritis & Rheumatism, 10(4), 357–376. https://doi.org/10.1002/art.1780100407

49. Namiki O, Toyoshima H, Morisaki N. Therapeutic effect of intra-articular injection of high molecular weight hyaluronic acid on osteoarthritis of the knee. International Journal of Clinical Pharmacology, Therapy, and Toxicology. 1982 Nov;20(11):501-507.

50. Termeer, C. C., Hennies, J., Voith, U., Ahrens, T., M. Weiss, J., Prehm, P., & Simon, J. C. (2000). Oligosaccharides of Hyaluronan Are Potent Activators of Dendritic Cells. The Journal of Immunology, 165(4), 1863–1870. https://doi.org/10.4049/jimmunol.165.4.1863

51. Ronca, F., Palmieri, L., Panicucci, P., & Ronca, G. (1998). Anti-inflammatory activity of chondroitin sulfate. Osteoarthritis and Cartilage, 6, 14–21. https://doi.org/10.1016/s1063-4584(98)80006-x

52. Tully, S. E., Mabon, R., Gama, C. I., Tsai, S. M., Liu, X., & Hsieh-Wilson, L. C. (2004). A Chondroitin Sulfate Small Molecule that Stimulates Neuronal Growth. Journal of the American Chemical Society, 126(25), 7736–7737. https://doi.org/10.1021/ja0484045

53. Bjornsson, T. D., Nash, P. V., & Schaten, R. (1982). The anticoagulant effect of chondroitin-4-sulfate. Thrombosis Research, 27(1), 15–21. https://doi.org/10.1016/0049-3848(82)90273-0

54. Powell, A. K., Fernig, D. G., & Turnbull, J. E. (2002). Fibroblast Growth Factor Receptors 1 and 2 Interact Differently with Heparin/Heparan Sulfate. Journal of Biological Chemistry, 277(32), 28554–28563. https://doi.org/10.1074/jbc.m111754200

55. Smith, G. F. (1977). The heparin-thrombin complex in the mechanism of thrombin inactivation by heparin. Biochemical and Biophysical Research Communications, 77(1), 111–117. https://doi.org/10.1016/s0006-291x(77)80171-x

56. Linhardt, R. J., & Liu, J. (2012). Synthetic heparin. Current Opinion in Pharmacology, 12(2), 217–219. https://doi.org/10.1016/j.coph.2011.12.002

57. Ruocco, N., Costantini, S., Guariniello, S., & Costantini, M. (2016). Polysaccharides from the Marine Environment with Pharmacological, Cosmeceutical and Nutraceutical Potential. Molecules, 21(5), 551. https://doi.org/10.3390/molecules21050551

58. Pomin, V. (2014). Holothurian Fucosylated Chondroitin Sulfate. Marine Drugs, 12(1), 232–254. https://doi.org/10.3390/md12010232

59. Berteau, O. (2003). Sulfated fucans, fresh perspectives: structures, functions, and biological properties of sulfated fucans and an overview of enzymes active toward this class of polysaccharide. Glycobiology, 13(6), 29R–40. https://doi.org/10.1093/glycob/cwg058

60. Aquino, R. S. (2004). Occurrence of sulfated galactans in marine angiosperms: evolutionary implications. Glycobiology, 15(1), 11–20. https://doi.org/10.1093/glycob/cwh138

61. Farias, W. R. L., Valente, A.-P., Pereira, M. S., & Mourão, P. A. S. (2000). Structure and Anticoagulant Activity of Sulfated Galactans. Journal of Biological Chemistry, 275(38), 29299–29307. https://doi.org/10.1074/jbc.m002422200

62. Mourão, P. A. S., Pereira, M. S., Pavão, M. S. G., Mulloy, B., Tollefsen, D. M., Mowinckel, M.-C., & Abildgaard, U. (1996). Structure and Anticoagulant Activity of a Fucosylated Chondroitin Sulfate from Echinoderm. Journal of Biological Chemistry, 271(39), 23973–23984. https://doi.org/10.1074/jbc.271.39.23973

63. Horst, R., Wider, G., Fiaux, J., Bertelsen, E. B., Horwich, A. L., & Wuthrich, K. (2006). Proton-proton Overhauser NMR spectroscopy with polypeptide chains in large structures. Proceedings of the National Academy of Sciences, 103(42), 15445–15450. https://doi.org/10.1073/pnas.0607141103

64. Jones, C. R., Greenhalgh, M. D., Bame, J. R., Simpson, T. J., Cox, R. J., Marshall, J. W., & Butts, C. P. (2016). Subtle temperature-induced changes in small molecule conformer dynamics – observed and quantified by NOE spectroscopy. Chemical Communications, 52(14), 2920–2923. https://doi.org/10.1039/c5cc10509a

65. Keepers, J. W., & James, T. L. (1984). A theoretical study of distance determinations from NMR. Two-dimensional nuclear overhauser effect spectra. Journal of Magnetic Resonance (1969), 57(3), 404–426. https://doi.org/10.1016/0022-2364(84)90257-9

66. Beddingfield, S. D., & McClintock, J. B. (2000). Demographic Characteristics of Lytechinus variegatus (Echinoidea: Echinodermata) from Three Habitats in a North Florida Bay, Gulf of Mexico. Marine Ecology, 21(1), 17–40. https://doi.org/10.1046/j.1439-0485.2000.00688.x

67. Cinelli, L. P., Vilela-Silva, A.-C. E. S., & Mourão, P. A. S. (2009). Seminal fluid from sea urchin (Lytechinus variegatus) contains complex sulfated polysaccharides linked to protein. Comparative Biochemistry and Physiology Part B: Biochemistry and Molecular Biology, 154(1), 108–112. https://doi.org/10.1016/j.cbpb.2009.05.004

68. Mourão, P. (1999). Searching for Alternatives to Heparin Sulfated Fucans from Marine Invertebrates. Trends in Cardiovascular Medicine, 9(8), 225–232. https://doi.org/10.1016/s1050-1738(00)00032-3

69. Xu, S.-Y., Huang, X., & Cheong, K.-L. (2017). Recent Advances in Marine Algae Polysaccharides: Isolation, Structure, and Activities. Marine Drugs, 15(12), 388. https://doi.org/10.3390/md15120388

70. Pomin, V. H., Valente, A. P., Pereira, M. S., & Mourão, P. A. S. (2005). Mild acid hydrolysis of sulfated fucans: a selective 2-desulfation reaction and an alternative approach for preparing tailored sulfated oligosaccharides. Glycobiology, 15(12), 1376–1385. https://doi.org/10.1093/glycob/cwj030

71. Bezerra, F. F., Vignovich, W. P., Aderibigbe, A. O., Liu, H., Sharp, J. S., Doerksen, R. J., & Pomin, V. H. (2020). Conformational properties of l-fucose and the tetrasaccharide building block of the sulfated l-fucan from Lytechinus variegatus. Journal of Structural Biology, 209(1), 107407. https://doi.org/10.1016/j.jsb.2019.107407

72. Pomin, V. H., Pereira, M. S., Valente, A.-P., Tollefsen, D. M., Pavão, M. S. G., & Mourão, P. A. S. (2004). Selective cleavage and anticoagulant activity of a sulfated fucan: stereospecific removal of a 2-sulfate ester from the polysaccharide by mild acid hydrolysis, preparation of oligosaccharides, and heparin cofactor II–dependent anticoagulant activity. Glycobiology, 15(4), 369–381. https://doi.org/10.1093/glycob/cwi021

73. Takeda, M., Jee, J., Ono, A. M., Terauchi, T., & Kainosho, M. (2009). Hydrogen Exchange Rate of Tyrosine Hydroxyl Groups in Proteins As Studied by the Deuterium Isotope Effect on CζChemical Shifts. Journal of the American Chemical Society, 131(51), 18556–18562. https://doi.org/10.1021/ja907911y

74. Halford, J. O., & Pecherer, B. (1938). Exchange of Deuterium Between Methanol and Water: Vibrations of the Hydroxyl Group in Methanol and Methanol-d: The Entropy of Methanol. The Journal of Chemical Physics, 6(10), 571–575. https://doi.org/10.1063/1.1750125

75. Brown, G. D., Bauer, J., Osborn, H. M. I., & Kuemmerle, R. (2018). A Solution NMR Approach To Determine the Chemical Structures of Carbohydrates Using the Hydroxyl Groups as Starting Points. ACS Omega, 3(12), 17957–17975. https://doi.org/10.1021/acsomega.8b02136

76. Palmer, A. G., III. (2014). Chemical exchange in biomacromolecules: Past, present, and future. Journal of Magnetic Resonance, 241, 3–17. https://doi.org/10.1016/j.jmr.2014.01.008

77. Sklenář, V., Brooks, B. R., Zon, G., & Bax, A. (1987). Absorption mode two-dimensional NOE spectroscopy of exchangeable protons in oligonucleotides. FEBS Letters, 216(2), 249–252. https://doi.org/10.1016/0014-5793(87)80699-3

78. Williamson, M. P. (2013). Using chemical shift perturbation to characterise ligand binding. Progress in Nuclear Magnetic Resonance Spectroscopy, 73, 1–16. https://doi.org/10.1016/j.pnmrs.2013.02.001

79. Zhou, G. -p. (2002). Characterization by NMR and molecular modeling of the binding of polyisoprenols and polyisoprenyl recognition sequence peptides: 3D structure of the complexes reveals sites of specific interactions. Glycobiology, 13(2), 51–71. https://doi.org/10.1093/glycob/cwg008

80. Post, C. (2003). Exchange-transferred NOE spectroscopy and bound ligand structure determination. Current Opinion in Structural Biology, 13(5), 581–588. https://doi.org/10.1016/j.sbi.2003.09.012

81. Groves, P., Kövér, K. E., André, S., Bandorowicz-Pikula, J., Batta, G., Bruix, M., Buchet, R., Canales, A., Cañada, F. J., Gabius, H.-J., Laurents, D. V., Naranjo, J. R., Palczewska, M., Pikula, S., Rial, E., Strzelecka-Kiliszek, A., & Jiménez-Barbero, J. (2007). Temperature dependence of ligand–protein complex formation as reflected by saturation transfer difference NMR experiments. Magnetic Resonance in Chemistry, 45(9), 745–748. https://doi.org/10.1002/mrc.2041

82. Aretz, J., & Rademacher, C. (2019). Ranking Hits From Saturation Transfer Difference Nuclear Magnetic Resonance–Based Fragment Screening. Frontiers in Chemistry, 7. https://doi.org/10.3389/fchem.2019.00215

83. Angulo, J., & Nieto, P. M. (2011). STD-NMR: application to transient interactions between biomolecules—a quantitative approach. European Biophysics Journal, 40(12), 1357–1369. https://doi.org/10.1007/s00249-011-0749-5

84. Teilum, K., Kunze, M. B. A., Erlendsson, S., & Kragelund, B. B. (2017). (S)Pinning down protein interactions by NMR. Protein Science, 26(3), 436–451. https://doi.org/10.1002/pro.3105

85. Yu, F., Roy, S., Arevalo, E., Schaeck, J., Wang, J., Holte, K., Duffner, J., Gunay, N. S., Capila, I., & Kaundinya, G. V. (2014). Characterization of heparin–protein interaction by saturation transfer difference (STD) NMR. Analytical and Bioanalytical Chemistry, 406(13), 3079–3089. https://doi.org/10.1007/s00216-014-7729-4

86. Bergeron, S. J., Henry, I. D., Santini, R. E., Aghdasi, A., & Raftery, D. (2008). Saturation transfer double-difference NMR spectroscopy using a dual solenoid microcoil difference probe. Magnetic Resonance in Chemistry, 46(10), 925–929. https://doi.org/10.1002/mrc.2275

87. Fehér, K., Groves, P., Batta, G., Jiménez-Barbero, J., Muhle-Goll, C., & Kövér, K. E. (2008). Competition Saturation Transfer Difference Experiments Improved with Isotope Editing and Filtering Schemes in NMR-Based Screening. Journal of the American Chemical Society, 130(50), 17148–17153. https://doi.org/10.1021/ja804468k

88. Deshauer, C., Morgan, A. M., Ryan, E. O., Handel, T. M., Prestegard, J. H., & Wang, X. (2015). Interactions of the Chemokine CCL5/RANTES with Medium-Sized Chondroitin Sulfate Ligands. Structure, 23(6), 1066–1077. https://doi.org/10.1016/j.str.2015.03.024

89. Linhardt, R. J. (2016). Heparin and anticoagulation. Frontiers in Bioscience, 21(7), 1372–1392. https://doi.org/10.2741/4462

90. Jin, L., Abrahams, J. P., Skinner, R., Petitou, M., Pike, R. N., & Carrell, R. W. (1997). The anticoagulant activation of antithrombin by heparin. Proceedings of the National Academy of Sciences, 94(26), 14683–14688. https://doi.org/10.1073/pnas.94.26.14683

91. HRICOVÍNI, M., GUERRINI, M., BISIO, A., TORRI, G., PETITOU, M., & CASU, B. (2001). Conformation of heparin pentasaccharide bound to antithrombin III. Biochemical Journal, 359(2), 265. https://doi.org/10.1042/0264-6021:3590265

92. Stancanelli, E., Elli, S., Hsieh, P.-H., Liu, J., & Guerrini, M. (2018). Recognition and Conformational Properties of an Alternative Antithrombin Binding Sequence Obtained by Chemoenzymatic Synthesis. ChemBioChem, 19(11), 1178–1188. https://doi.org/10.1002/cbic.201800095

93. Guerrini, M., Elli, S., Mourier, P., Rudd, T. R., Gaudesi, D., Casu, B., Boudier, C., Torri, G., & Viskov, C. (2012). An unusual antithrombin-binding heparin octasaccharide with an additional 3-O-sulfated glucosamine in the active pentasaccharide sequence. Biochemical Journal, 449(2), 343–351. https://doi.org/10.1042/bj20121309

94. Janssens, R., Struyf, S., & Proost, P. (2017). The unique structural and functional features of CXCL12. Cellular & Molecular Immunology, 15(4), 299–311. https://doi.org/10.1038/cmi.2017.107

95. Friand, V., Haddad, O., Papy-Garcia, D., Hlawaty, H., Vassy, R., Hamma-Kourbali, Y., Perret, G.-Y., Courty, J., Baleux, F., Oudar, O., Gattegno, L., Sutton, A., & Charnaux, N. (2009). Glycosaminoglycan mimetics inhibit SDF-1/CXCL12-mediated migration and invasion of human hepatoma cells. Glycobiology, 19(12), 1511–1524. https://doi.org/10.1093/glycob/cwp130

96. Laguri, C., Sapay, N., Simorre, J.-P., Brutscher, B., Imberty, A., Gans, P., & Lortat-Jacob, H. (2011). 13C-Labeled Heparan Sulfate Analogue as a Tool To Study Protein/Heparan Sulfate Interactions by NMR Spectroscopy: Application to the CXCL12α Chemokine. Journal of the American Chemical Society, 133(25), 9642–9645. https://doi.org/10.1021/ja201753e

97. MURAMATSU, T. (2010). Midkine, a heparin-binding cytokine with multiple roles in development, repair and diseases. Proceedings of the Japan Academy, Series B, 86(4), 410–425. https://doi.org/10.2183/pjab.86.410

98. Solera, C., Macchione, G., Maza, S., Kayser, M. M., Corzana, F., de Paz, J. L., & Nieto, P. M. (2016). Chondroitin Sulfate Tetrasaccharides: Synthesis, Three-Dimensional Structure and Interaction with Midkine. Chemistry - A European Journal, 22(7), 2356–2369. https://doi.org/10.1002/chem.201504440

99. Iwasaki, W. (1997). Solution structure of midkine, a new heparin-binding growth factor. The EMBO Journal, 16(23), 6936–6946. https://doi.org/10.1093/emboj/16.23.6936

100. Juremalm, M., Olsson, N., & Nilsson, G. (2002). Selective CCL5/RANTES-induced mast cell migration through interactions with chemokine receptors CCR1 and CCR4. Biochemical and Biophysical Research Communications, 297(3), 480–485. https://doi.org/10.1016/s0006-291x(02)02244-1

101. Couper, K. N., Blount, D. G., & Riley, E. M. (2008). IL-10: The Master Regulator of Immunity to Infection. The Journal of Immunology, 180(9), 5771–5777. https://doi.org/10.4049/jimmunol.180.9.5771

102. Stopschinski, B. E., Holmes, B. B., Miller, G. M., Manon, V. A., Vaquer-Alicea, J., Prueitt, W. L., Hsieh-Wilson, L. C., & Diamond, M. I. (2018). Specific glycosaminoglycan chain length and sulfation patterns are required for cell uptake of tauversusα-synuclein and β-amyloid aggregates. Journal of Biological Chemistry, 293(27), 10826–10840. https://doi.org/10.1074/jbc.ra117.000378

103. Künze, G., Köhling, S., Vogel, A., Rademann, J., & Huster, D. (2015). Identification of the Glycosaminoglycan Binding Site of Interleukin-10 by NMR Spectroscopy. Journal of Biological Chemistry, 291(6), 3100–3113. https://doi.org/10.1074/jbc.m115.681759

104. LeVea, C., & Mooney, R. (2003). The Leukocyte Common Antigen-Related Protein LAR: Candidate PTP for Inhibitory Targeting. Current Topics in Medicinal Chemistry, 3(7), 809–819. https://doi.org/10.2174/1568026033452294

105. Fisher, D., Xing, B., Dill, J., Li, H., Hoang, H. H., Zhao, Z., Yang, X.-L., Bachoo, R., Cannon, S., Longo, F. M., Sheng, M., Silver, J., & Li, S. (2011). Leukocyte Common Antigen-Related Phosphatase Is a Functional Receptor for Chondroitin Sulfate

Proteoglycan Axon Growth Inhibitors. Journal of Neuroscience, 31(40), 14051–14066. https://doi.org/10.1523/jneurosci.1737-11.2011

106. Fox, A. N., & Zinn, K. (2005). The Heparan Sulfate Proteoglycan Syndecan Is an In Vivo Ligand for the Drosophila LAR Receptor Tyrosine Phosphatase. Current Biology, 15(19), 1701–1711. https://doi.org/10.1016/j.cub.2005.08.035

107. Gao, Q., Yang, J.-Y., Moremen, K. W., Flanagan, J. G., & Prestegard, J. H. (2018). Structural Characterization of a Heparan Sulfate Pentamer Interacting with LAR-Ig1-2. Biochemistry, 57(15), 2189–2199. https://doi.org/10.1021/acs.biochem.8b00241

108. Zhang, F., Zheng, L., Cheng, S., Peng, Y., Fu, L., Zhang, X., & Linhardt, R. J. (2019). Comparison of the Interactions of Different Growth Factors and Glycosaminoglycans. Molecules, 24(18), 3360. https://doi.org/10.3390/molecules24183360

109. Yun, Y.-R., Won, J. E., Jeon, E., Lee, S., Kang, W., Jo, H., … Kim, H.-W. (2010). Fibroblast Growth Factors: Biology, Function, and Application for Tissue Regeneration. Journal of Tissue Engineering, 1(1), 218142. https://doi.org/10.4061/2010/218142

APPENDICES

APPENDIX I

Pomin, V. H., **Vignovich, W. P.,** Gonzales, A. V., Vasconcelos, A. A., & Mulloy, B. (2019). Galactosaminoglycans: Medical Applications and Drawbacks. Molecules, 24(15), 2803. https://doi.org/10.3390/molecules24152803

Included as Supplementary File

APPENDIX II

Bezerra, F. F., **Vignovich, W. P**., Aderibigbe, A. O., Liu, H., Sharp, J. S., Doerksen, R. J., & Pomin, V. H. (2020). Conformational properties of l-fucose and the tetrasaccharide building block of the sulfated l-fucan from *Lytechinus variegatus*. Journal of Structural Biology, 209(1), 107407. https://doi.org/10.1016/j.jsb.2019.107407

Included as Supplementary File

APPENDIX III

Vignovich W.P., Pomin, V.H. (2020). Saturation Transfer Difference in Characterization of Glycosaminoglycan-Protein Interactions. SLAS Technology, accepted waiting for publishment

Included as Supplementary File

VITA

Work Address
Faser 455
Department of BioMolecular Sciences
University of Mississippi
University, MS 38677

Education

BSc. Southern Illinois University 2013-2017
Bachelor of Science Major: Plant Biology, Specialization in Molecular and Biochemical Physiology

Awards

James E. Ozment Achievement Award in Natural History 2016

Work Experience

Undergraduate Research Assistant 2014-2015
Southern Illinois University Herbarium curated by Dr. Nancy Garwood
Department of Plant Biology Southern Illinois University

Undergraduate Research Assistant 2015-2016
Dr. Kurt Neubig Plant Systematics Laboratory
Department of Plant Biology Southern Illinois University

Undergraduate Research Assistant 2016-2017
Dr. David Lightfoot Biotechnology and Genomics Laboratory
Department of Plant Biology and Agriculture Southern Illinois University

Graduate Research Assistant 2018-Present
Dr. Vitor Pomin Biomolecular NMR Laboratory
Division of Pharmacognosy, Department of Biomolecular Sciences, The University of Mississippi